A Review of Gas-Surface Interaction Models for Orbital Aerodynamics Applications

Sabrina Livadiotti*[a], Nicholas H. Crisp[a], Peter C.E. Roberts[a], Stephen D. Worrall[a], Vitor T.A. Oiko[a], Steve Edmondson[a], Sarah J. Haigh[a], Claire Huyton[a], Katharine L. Smith[a], Luciana A. Sinpetru[a], Brandon E. A. Holmes[a], Jonathan Becedas[b], Rosa María Domínguez[b], Valentín Cañas[b], Simon Christensen[c], Anders Mølgaard[c], Jens Nielsen[c], Morten Bisgaard[c], Yung-An Chan[d], Georg H. Herdrich[d], Francesco Romano[d], Stefanos Fasoulas[d], Constantin Traub[d], Daniel Garcia-Almiñana[e], Silvia Rodriguez-Donaire[e], Miquel Sureda[e], Dhiren Kataria[f], Badia Belkouchi[g], Alexis Conte[g], Jose Santiago Perez[g], Rachel Villain[g] and Ron Outlaw[h]

[a]*The University of Manchester, Oxford Road, Manchester, M13 9PL, United Kingdom*
[b]*Elecnor Deimos Satellite Systems, Calle Francia 9, 13500 Puertollano, Spain*
[c]*GomSpace AS, Langagervej 6, 9220 Aalborg East, Denmark*
[d]*University of Stuttgart, Pfaffenwaldring 29, 70569 Stuttgart, Germany*
[e]*UPC-BarcelonaTECH, Carrer de Colom 11, 08222 Terrassa, Barcelona, Spain*
[f]*Mullard Space Science Laboratory (UCL), Holmbury St. Mary, Dorking, RH5 6NT, United Kingdom*
[g]*Euroconsult, 86 Boulevard de Sébastopol, 75003 Paris, France*
[h]*Christopher Newport University Engineering, Newport News, Virginia 23606, United States*

Abstract

Renewed interest in Very Low Earth Orbits (VLEO) - i.e. altitudes below 450 km - has led to an increased demand for accurate environment characterisation and aerodynamic force prediction. While the former requires knowledge of the mechanisms that drive density variations in the thermosphere, the latter also depends on the interactions between the gas-particles in the residual atmosphere and the surfaces exposed to the flow. The determination of the aerodynamic coefficients is hindered by the numerous uncertainties that characterise the physical processes occurring at the exposed surfaces. Several models have been produced over the last 60 years with the intent of combining accuracy with relatively simple implementations. In this paper the most popular models have been selected and reviewed using as discriminating factors relevance with regards to orbital aerodynamics applications and theoretical agreement with gas-beam experimental data. More sophisticated models were neglected, since their increased accuracy is generally accompanied by a substantial increase in computation times which is likely to be unsuitable for most space engineering applications. For the sake of clarity, a distinction was introduced between *physical* and *scattering kernel theory* based gas-surface interaction models. The *physical* model category comprises the Hard Cube model, the Soft Cube model and the Washboard model, while the *scattering kernel* family consists of the Maxwell model, the Nocilla-Hurlbut-Sherman model and the Cercignani-Lampis-Lord model. Limits and assets of each model have been discussed with regards to the context of this paper. Wherever possible, comments have been provided to help the reader to identify possible future challenges for gas-surface interaction science with regards to orbital aerodynamic applications.

Keywords: Gas-Surface Interaction, Very Low Earth Orbit, Orbital Aerodynamics

Difficulties in modelling the interaction of the near-Earth aerodynamic environment with satellites in Low Earth Orbit (LEO) are due to a lack of knowledge on the mechanisms that determine the thermosphere total density variation, the magnitude and the direction of the thermospheric wind vector and the dynamics of the Gas-Surface Interaction (GSI). These uncertainties affect the computation of the acceleration that drag - the main source of perturbation for altitudes below 600 km [1] - exerts on satellites:

$$\mathbf{a_D} = -\frac{1}{2}\rho V_{rel}^2 \frac{C_D S_{ref}}{m} \frac{\mathbf{V_{rel}}}{|\mathbf{V_{rel}}|} \tag{1}$$

where S_{ref} is the reference surface adopted to perform the computation and m is the satellite's mass, often the only parameter known with substantial accuracy unless any propellant consumption needs to be acknowledged. In Eq. 1 uncertainties are found in the assessment of the total density (ρ), the aerodynamic drag coefficient (C_D) and the satellite velocity with regards to the rotating atmosphere ($\mathbf{V_{rel}}$). Since these sources of uncertainties are mutually linked, any attempt to discuss them separately is improper. However, the complexity of the problem demands some form of simplification. Therefore, challenges encountered in estimating ρ and $\mathbf{V_{rel}}$, whose variations are generally associated with fluctuations in the thermosphere environment, will not be treated in this review. Consequently, the key factors that for a given velocity of the flow contribute to determination of the dynamic pressure q (Eq. 2) will be disregarded to devote more attention to those engineering variables that can be modified through proper design and materials selection:

$$q(t) = \frac{1}{2}\rho(t)V_{rel}(t)^2 \tag{2}$$

For the reader's knowledge, comprehensive works covering the mechanisms affecting the estimate of dynamic pressure can be found in [2–8].

In the following sections of this paper, the effect of GSI dynamics on drag evaluation and computation of the aerodynamic coefficients will be discussed. Some information regarding the aerodynamic regime experienced by satellites in LEO - and especially in Very Low Earth Orbit (VLEO) - will be provided in an attempt to create an adequate background for the discussion. Attention will be focused on statistical and physical GSI models which have obtained considerable success both in engineering applications and surface science for their capability to describe the complex processes occurring at the surface with relative simplicity. In this regard, the intention is to create continuity with a recent review paper on the topic by Mostaza Prieto et al. [9], which focuses on classical analytical models used for aerodynamic computation in LEO. Gas-beam experimental results conducted in the physical regimes of interest for this paper will finally be presented, and the behaviour of the models described will be discussed, wherever possible, against the identified trends in scattering. The objective is thus to highlight the points of strength and the limits of the theoretical models against the available experimental data. In this way possible feature developments can be discussed and hopefully a reasonable picture of the difficulties encountered in approaching the GSI problem for orbital aerodynamics can be provided.

Increased knowledge of the interaction mechanisms occurring in the gas-solid phase system is crucial not only for scientific achievement, but also for the possibility of improving aerodynamic performance of spacecraft operating in VLEO [10, 11]. This would reflect in increased confidence in assessing the advantages and the drawbacks of employing aerodynamic torques for orbit [12–18] and attitude control purposes [19–28]. Overestimating or underestimating the aerodynamic torques induced by the actuation of aerodynamic control surfaces has an impact on

2

the altitude range for which aerodynamic manoeuvring is expected to be feasible. This seems relevant especially for missions operating in periods of low solar activity, when the thermospheric density values at altitudes above 200 km are significantly lower than those expected during high solar activity [9]. In terms of attitude control implementation, the achievable aerodynamic control authority about the roll, pitch and yaw body axes drives the design of the controller selected. This is especially true if conventional actuators (e.g. reaction wheels, magnetorquers) are meant to be used in synergy with the designated control surfaces. Undesired aerodynamic torques may counteract the control action of the wheels, disturbing the attitude task and eventually leading to saturation. Similarly, aerodynamic orbit control [29], formation flying [30–33] and rendezvous manoeuvres [34, 35] would significantly benefit from any improvement in GSI models, especially with regards to the possibility of producing control torques in the direction perpendicular to the orbit plane. A reliable estimation of the aerodynamic coefficients is also fundamental in the evaluation of the impact that aerodynamic based manoeuvres may have on the rate of decay of satellites in orbit. This knowledge could potentially be useful for a better prediction of the satellite re-entry trajectory [16, 18] or to achieve a better knowledge of the expected aerodynamic forces and torques induced on the ram surfaces during controlled re-entry in atmosphere. This knowledge represents a considerable advantage even for spacecraft that are already in orbit, assuming that the materials employed for the external surfaces are known and that a good prediction of the environmental conditions is achivable. Nevertheless, a better knowledge of the phenomena occuring at the surface could potentially drive a more rational design of the satellite geometry according to the desired aerodynamic performances. The same geometry is indeed expected to provide a different aerodynamic behaviour with varying scattering re-emission patterns. Comparably, the design of Atmospheric Breathing Electric Propulsion (ABEP) systems is driven by the aerodynamic performance expected for the materials employed [36]. Any improvements in the reliability of the GSI models may translate in a more confident definition of optimal performance ranges and it can possibly pave the way for new design criteria.

1. The Aerodynamic Environment

At the altitudes where VLEO satellites orbit, i.e. below 450 km [37], the atmosphere is so tenuous that the flow can no longer be considered a continuum. In this scenario, the principles that rule the interaction of gas constituents with each other and with a body immersed in the flow change, as do the assumptions used to investigate the aerodynamic environment. The discriminating factor employed to distinguish between the different regimes is a dimensionless ratio known as the Knudsen number (K_n), which compares the order of magnitude of the molecular mean free path (λ) with a characteristic dimension of the flow field (L):

$$K_n = \frac{\lambda}{L} \tag{3}$$

As evidenced by the definition, the Knudsen number is not strictly a flow property since its value is partially controlled by the reference length adopted to describe the field of motion. L is generally assumed to coincide with a significant dimension of a body in the flow, but this association is not unique. Between λ and ρ there is an inverse proportional correlation, according to which, high values of the mean free path (and thus K_n) are usually associated with low density levels or gas-surface interactions occurring at nano-scale length.

Three fundamentals regimes are usually identified according to the Knudsen number. Small K_n ($0 < K_n < 0.1$) are typical of the familiar continuum dynamics, where collisions between particles is the prevalent mechanism of interaction. When $K_n \rightarrow \infty$, the length travelled by the particles before impingement with other particles in the gas mixture is considerable compared to the characteristic flow-field dimension. In these conditions, the flow is characterised by a structure in which the interaction of the gas-particles with the surface dominates over inter-particle collisions. The distance a reflected particle travels before colliding with the free stream is of the same order of magnitude of λ and consequently, the flow itself can be considered collisionless. In these conditions, it can be assumed that the presence of a body in the flow-field does not perturb the distribution of the incident stream of particles in the vicinity of the body itself, and consequently, no shock waves are expected to arise. This behaviour is typical of a highly rarefied flow regime, more commonly known as *free molecular flow* (FMF). The majority of authors agree to set $K_n > 10$ as the lower limit to identify this region [9, 27, 38–42], with some variations [43]. Intermediate K_n values identify the near-free molecular regime ($K_n \gg 1$) and the complex transitional regime ($K_n \sim 1$), where continuum and rarefied dynamics phenomena are of similar relevance [44].

The determination of the Knudsen number for the orbital aerodynamics problem is especially dependent on a judicious choice of the mean free path for the coordinate system used. For the free molecular assumption to be valid, 1) the interactions of the incident particles with each other and 2) the interactions of the incident particles with the reflected particles should be negligible compared to the probability of collision of the incident particles with the surface. For conditions 1) and 2) to be met simultaneously, it is necessary that the order of magnitude of the associated mean free paths is such that:

$$K_{n,\lambda_{ii}} = \frac{\lambda_{ii}}{L} > 10 \qquad K_{n,\lambda_{ir}} = \frac{\lambda_{ir}}{L} > 10 \tag{4}$$

where λ_{ii} is the mean free path referring to the interaction with other incident particles and λ_{ir} is the mean free path related to the interaction with the reflected particles. According to its definition in kinetic theory, the mean free path is inversely proportional to the effective collision cross-sectional area (πd^2) and the number density of the particles (n) [40]:

$$\lambda \propto \frac{1}{\pi d^2 n} \tag{5}$$

where d is the radius of the sphere of influence. For the problem examined, the velocity of the satellite through the gas is considerable and the re-emission of the particles from the surface is typically thermal. In these conditions, the number density of the reflected molecules can significantly increase, especially in proximity of the surface, possibly changing the nature of the flow locally. If the coordinate system is assumed to be fixed with the body immersed in the flow, λ_{ir} tends to be an order of magnitude smaller than λ_{ii} [40] and should thus be preferred for a conservative estimation of K_n. For many applications, however, the free stream mean free path (λ_∞), defined with regards to a coordinate system fixed with the gas, is adopted:

$$\lambda_\infty = \frac{1}{\sqrt{2}\pi d^2 n_i} \tag{6}$$

where n_i is the number density of the free stream incident particles. The relation between λ_{ir} and λ_∞ is provided by Sentman [40]:

$$\lambda_{ir} = \sqrt{\frac{\pi}{2}} \frac{1}{s} \sqrt{\frac{T_r}{T_i}} \lambda_\infty \tag{7}$$

where s is the molecular speed ratio defined later in this section, T_r is the temperature of the reflected particles and T_i is the temperature of the incident particles. Generally for satellites in VLEO, $s > 5$ and $T_r/T_i < 1$. As a consequence, λ_∞ can be considerably bigger that λ_{ir}. Results shown by Walker et al. [45] suggest that the K_n number referred to freestream should be in the order of 10^3 to assure overall free molecular conditions. Detailed analysis of the uncertainties related to the K_n number computation for orbital aerodynamics applications is provided in [40].

Because of the extremely low density of the upper atmosphere, VLEO is generally characterised as a FMF environment. While the Knudsen number defines the degree of rarefaction of the gas, another parameter is needed to indicate how the relative magnitude of the satellite's velocity and the most probable gas velocity affects the aerodynamics. Just as the Mach number expresses the relationship between the body's macroscopic velocity and the speed of sound, the molecular speed ratio indicates the ratio between the gas macroscopic velocity (v_m) and the most probable molecular thermal velocity (v_t) according to a Maxwell-Boltzmann distribution:

$$s = \frac{v_m}{v_t} = \frac{V_\infty}{\sqrt{\frac{2RT_\infty}{m_m}}} \tag{8}$$

In Eq. 8, R is the gas constant, m_m is the gas molecular mass and T_∞ is the gas kinetic temperature of the free stream. For the orbital aerodynamics problem, the velocity of the body immersed in the FMF is so high that the investigation concerns the motion of a body travelling at high speeds through a gas at rest. Consequently, in Eq. 8 the gas macroscopic velocity effectively corresponds to the satellite's velocity (V_∞) and the two can be used interchangeably.

At a certain altitude, variations in thermal velocity - and thus internal energy - occur with alterations in the amount of energy absorbed by the atmosphere [4, 46, 47]. In these conditions, the random thermal velocity may play a role in the determination of the induced aerodynamic forces. This behaviour is generally associated with small values of s and the FMFs are accordingly referred as *hypothermal* flows.

On the contrary, when $s \to \infty$, the effect of the bulk velocity of the particles on the aerodynamic forces estimation is considered predominant. Under these conditions, the flow is said to be *hyperthermal* and approximate kinetic theories ignoring the drift caused by the random thermal motion of the particles are usually preferred. Typical values of s at VLEO altitudes are greater than 5. For general applications, the hyperthermal assumption is considered valid for $s > 5$ [9, 27] and, for this reason, it is frequently employed.

The particulate flow impinges on the external surfaces of a spacecraft, generating induced aerodynamic forces whose magnitude is only dependent on the nature of the interaction. The aerodynamic forces experienced by the satellite in the body-axes reference system conventionally used for flight-mechanics applications can be modelled referring to the familiar expression:

$$\mathbf{F_{aero}} = m\mathbf{a} = \frac{1}{2}\rho \, V_{rel}^2 S_{ref}\mathbf{C_F} \tag{9}$$

where, similarly to Eq.1, ρ is the thermospheric density, V_{rel} is the satellite velocity with regards to the oncoming flow, S_{ref} is the selected reference surface and $\mathbf{C_F} = [C_A, C_S, C_N]^T$ is the vector of the three aerodynamic components along the axial, the side and the normal direction,

5

respectively. Similarly, the resulting aerodynamic torques referenced to the centre of mass are given by:

$$\mathbf{T_{aero}} = \mathbf{r_{PO}} \times m\mathbf{a} = \frac{1}{2}\rho V_{rel}^2 S_{ref} l_{ref} \mathbf{C_M} \tag{10}$$

where $\mathbf{C_M} = [C_l, C_m, C_n]^T$ is the vector of the roll, pitch and yaw momentum coefficients and $\mathbf{r_{PO}}$ is the position vector defining the distance between the aerodynamic centre of pressure and the centre of mass. The magnitude of the aerodynamic forces and coefficients has been estimated in literature for bodies of different shapes making use of both analytical [41, 48–51] and numerical techniques [52, 53]. Both approaches have benefits and drawbacks and, ideally, the most advantageous strategy would be to adopt them in synergy, when permitted.

Regardless of the simulation technique, the estimation of the aerodynamic coefficients relies on the models employed to physically describe the underlying mechanism for GSI. $\mathbf{C_F}$ and $\mathbf{C_M}$ are generally computed extending the integrals of the local stress coefficients (c_F) to the surface exposed to the incident flow:

$$\mathbf{C_F} = \int_S \mathbf{c_F} \, dS \tag{11}$$

$$\mathbf{C_M} = \int_S \mathbf{r_{PO}} \times \mathbf{c_F} \, dS = \int_S (\mathbf{r_P} - \mathbf{r_O}) \times \mathbf{c_F} \, dS \tag{12}$$

The variety of proposed GSI models translates into a variety in c_F formulations. In particular, the expressions found in literature suggest that the aerodynamic coefficients are a complex function of a number of parameters which, once again, vary with the model adopted (Fig. 1 and 2). A certain agreement is however found in the use of the so-called accommodation coefficients, the wall temperature which is usually assumed constant, the incident gas kinetic temperature and the molecular speed ratio s. These parameters are likely to depart from their initial value with variations in surface contamination, composition and structure, surface thermal properties and incident particle energy and velocity. Further dependencies on geometry and velocity vector direction are incorporated by the components of stress acting perpendicularly and tangentially to the surface.

The incident free stream, assumed to be in local Maxwellian equilibrium, interacts with the surface transferring both energy and momentum to it. Kinetic theory-based GSI models try to describe the physics underlying this phenomenon according to the contribution coming from both the incident and re-emitted stream of particles, with major difficulties found in establishing a satisfactory mathematical model for the latter. The amount of energy and momentum exchanged is a measure of the equilibrium the impinging particles achieve with the surface before re-emission. Both phenomena are described by means of a set of average phenomenological coefficients. The *thermal* or *energy accommodation coefficient*, first introduced by Knudsen [54]:

$$\alpha_T = \frac{E_i - E_r}{E_i - E_w} = \frac{T_{k,i} - T_{k,r}}{T_{k,i} - T_w} \tag{13}$$

describes the energy exchange, assuming that the translational, rotational and vibrational energies of the particles are all affected to the same degree by the interaction with the wall [43]. In Eq. 13, E_i and E_r are the kinetic energies carried by the incident and the scattered fluxes, while E_w denotes the energy that would be carried away from the surface by the scattered flux if complete thermal equilibrium was achieved and particles were re-emitted according to a Maxwellian

6

distribution corresponding to the surface temperature (T_w). Similarly, $T_{k,i}$ and $T_{k,r}$ indicate the kinetic temperatures of the incident and reflected streams. In accordance to what will be discussed in the following sections, it is also appropriate to introduce a *partial thermal accommodation coefficient* [55], whose value depends on the specific incident (θ_i) and scattering (θ_r) directions selected with regards to the normal to the surface:

$$\alpha_{T,P}(\theta_i, \theta_r) = \frac{E_i(\theta_i) - E_r(\theta_r)}{E_i(\theta_i) - E_w} \tag{14}$$

To describe the momentum exchange, it is common practice to refer to the momentum coefficient (σ) [56]. Better physical correlation is usually achieved by adopting two separate accommodation coefficients to describe the normal (σ_n) and the tangential (σ_t) momentum exchange [43]:

$$\sigma_n = \frac{p_i - p_r}{p_i - p_w} \tag{15}$$

$$\sigma_t = \frac{\tau_i - \tau_r}{\tau_i} \qquad \tau_w = 0 \tag{16}$$

The quantities in Eq. 15 and 16 are analogous to those already described for α_T, the only difference being that in this case they refer to the momentum rather than the energy of the fluxes. The information of most significant value provided by α_T, σ_n and σ_t is that the distribution of the re-emitted particles and velocity is deeply influenced by the degree of accommodation of the incident molecules with the surface. By referring to these quantities, two classical and extreme mechanisms of interaction are identified, namely specular reflection and diffuse re-emission. If specular reflection occurs without any thermal accommodation, the molecules are elastically reflected, no thermal energy is transferred to the body and momentum exchange occurs only along the normal to the surface ($\alpha_T = \sigma_n = \sigma_t = 0$). The angle that the velocity vector of the reflected particles form with the surface is equal to the one of the incident stream and it lies in the same plane of the incident velocity vector and the normal to the surface (Fig.3, left).
If isothermal diffuse re-emission with complete thermal accommodation occurs ($\alpha_T = \sigma_n = \sigma_t = 1$), particles have time to reach equilibrium with the surface and they are re-emitted according to a probabilistic velocity and direction distribution determined by the wall temperature, regardless of the incident stream's history (Fig.3, right). Experimental results discussed in Section 4 however suggest that more complex scattering interactions are expected to occur at the surface.

In VLEO, solar emissions in the Extremely Ultra Violet (EUV) wavelength have sufficient energy to generate Atomic Oxygen (AO) from the diassociation of O_2. The chances for the high reactive AO to reassociate to form O_2 or O_3 are quite low because of the very large mean free path characterising extremely rarefied flow regimes. Because of this, AO represents the main atmospheric constituent at VLEO altitudes and the main source of contamination and degradation of surfaces exposed to the flow. Effects of AO interaction with polymers and metals include oxygen erosion and inclusion, as well as formation of volatile and non-volatile reaction products [57]. Because of the high degree of contamination of the surfaces in VLEO, most works assume diffuse reflection with complete thermal accommodation. However, if highly accommodated particles are likely to be predominant below 300 km [58], the same cannot be said at higher altitudes, where the atmosphere gradually becomes less and less dense, thus limiting the contaminant adsorption to the spacecraft surfaces. According to this, Moe and Moe [58] proposed a Maxwellian-like model to compute the drag coefficient. The latter uses a modified form

7

Parameters	S&C	Schamberg	Cook	Sentman	Maxwell	NHS	CLL	Hard Cube	Soft Cube	Washboard
Incidence angle [1]	●		●			●		●		●
Re-emission angle [1]						●				
Molecular speed ratio [2]	●			●		●				
Surface temperature [2]	●	◇	●	●	●	●	●	●	●	●
Free-stream temperature [2]	●	◇	●	●	◇	◇	◇	●	◇	◇
Incident particle energy [2]	◇	◇	◇	◇	◇	◇	◇	◇	◇	●
Normal momentum accommodation coefficient [3]	●									
Tangential momentum accommodation coefficient [3]	●						●			
Momentum accommodation coefficient [3]					●					
Normal energy accommodation coefficient [3]							●			
Thermal accommodation coefficient [3]		◇	●	●	◇	●				
Re-emission beam width parameter [4]		●								
Re-emission lobe shape function [4]		●								
Velocity of the reflected particles [5]		●	●	◇	●	●	●			
Velocity of the incident particles [5]	◇	●	●	◇	●	●	●	◇	◇	◇
Potential well-depth [6]									●	●
Range of interaction [6]									●	
Oscillatory frequency of surface atoms [6]									●	
Corrugation strength parameter [6]										●
Gas particle-surface atom mass ratio [7]								●	●	●
Mean molecular mass [7]	◇	◇	◇	◇	◇	◇	◇	◇	◇	◇

Column groups: **Common** (S&C, Schamberg, Cook, Sentman); **Kernels** (Maxwell, NHS, CLL); **Physical** (Hard Cube, Soft Cube, Washboard)

Figure 1: GSI models compared: parameters of dependence for scattering distributions and aerodynamic coefficients. Black dots are used to identify parameters explicitly declared in the formulations, while white rhombus indicate implicit parameters of dependence. Parameters are grouped according to the following families: [1] flow angles; [2] energy parameters; [3] accommodation coefficients; [4] beam shape parameters; [5] velocities; [6] interaction parameters; [7] mass parameters.
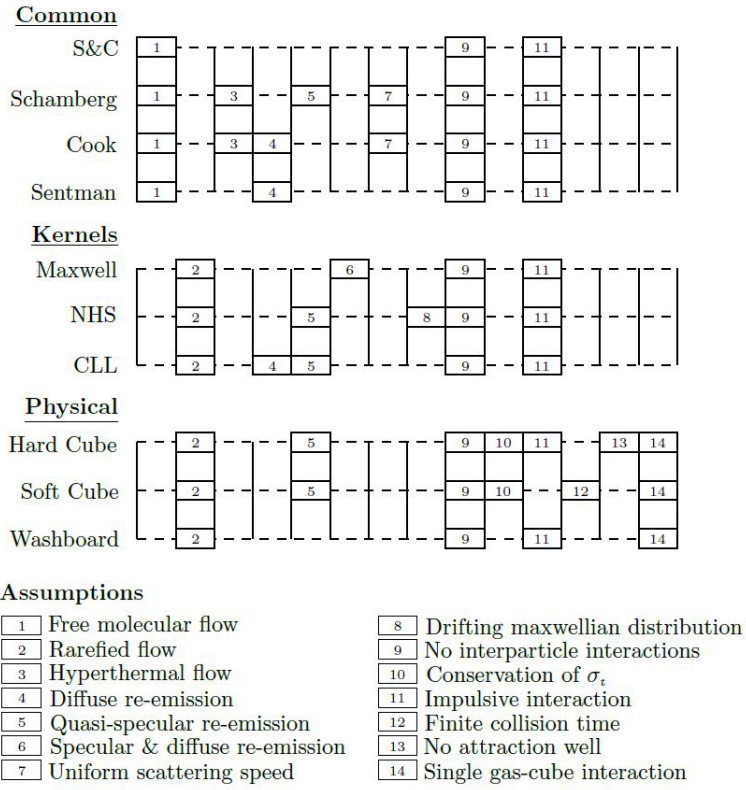
Common

S&C	1					9	11	
Schamberg	1	3	5	7		9	11	
Cook	1	3	4	7		9	11	
Sentman	1	4				9	11	

Kernels

Maxwell	2	6			9	11	
NHS	2	5	8	9	11		
CLL	2	4	5	9	11		

Physical

Hard Cube	2	5	9	10	11	13	14	
Soft Cube	2	5	9	10	12	14		
Washboard	2	9	11	14				

Assumptions

1	Free molecular flow	8	Drifting maxwellian distribution
2	Rarefied flow	9	No interparticle interactions
3	Hyperthermal flow	10	Conservation of σ_t
4	Diffuse re-emission	11	Impulsive interaction
5	Quasi-specular re-emission	12	Finite collision time
6	Specular & diffuse re-emission	13	No attraction well
7	Uniform scattering speed	14	Single gas-cube interaction

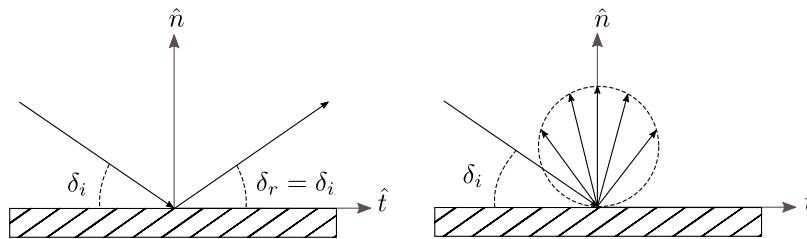Figure 2: Comparison between GSI models assumptions.

Figure 3: Mechanisms of re-emission for specular reflection without thermal accommodation (left) and diffuse reflection with complete thermal accommodation (right).
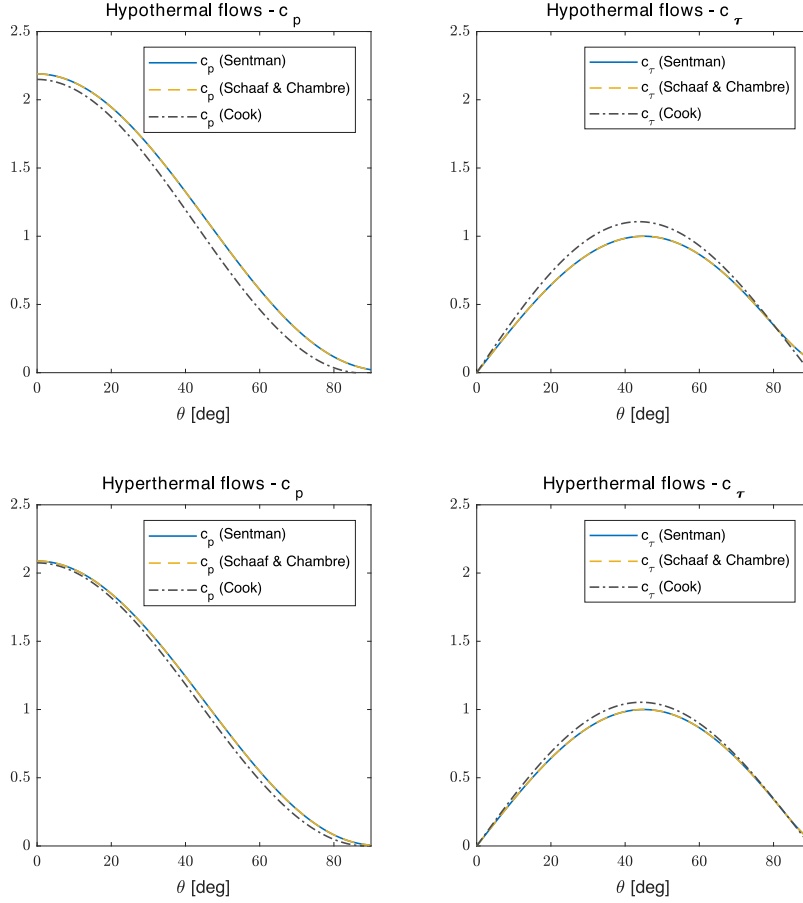
9

Figure 4: Comparison between Sentman's [40], Cook's [61] and Schaaf & Chambre's [43] model for hypothermal flows ($s = 6$) and hyperthermal flows ($s = 12$). The values of c_p and c_τ predicted by the models are shown, assuming $\alpha_T = 1$, $\sigma_n = 1$, $\sigma_t = 1$, $T_w = 300$ K and $T_\infty = 1000$ K and a flat plate as reference geometry.

of Sentman's model to compute the contribution associated with the $0 < \sigma < 1$ fraction of particles which are diffusely re-emitted. Schamberg's model [59] is instead used in combination with Goodman's accommodation coefficient [60] to address the input coming from the $(1 - \sigma)$ fraction that is quasi-specularly reflected. Schamberg's [59] and Sentman's [40] are probably the most popular models adopted to perform the estimation of aerodynamic properties. However, like many other GSI models, they rely on a specific set of assumptions that restrict their range of applicability. Schamberg's quasi-specular model assumes hyperthermal impinging FMF and uniform scattering speed along all directions. The hyperthermal approximation, conserved by Cook in a re-adaption of the model [61], provides valid results for applications in VLEO. However some care must be taken since, as more rigorously discussed in [40], neglecting the particle thermal velocity may introduce some errors for small angles of attack even for $s > 5$.

The effect of neglecting particle thermal velocity is more visible when the aerodynamic co-

efficients are expressed in terms of normal $\left(c_p\right)$ and shear (c_τ) stress components:

$$C_D \approx c_p cos\theta + c_\tau sin\theta \tag{17}$$

$$C_L \approx c_p sin\theta - c_\tau cos\theta \tag{18}$$

Fig. 4 shows the aerodynamic behaviour of a flat plate immersed in free molecular flow, according to a hyperthermal model (Cook [61]) and non-hyperthermal models (Schaaf & Chambre [43], Sentman [40]). For varying molecular speed ratios, variations of c_τ are noticeable for $\theta \sim 90°$, and thus grazing angles of attack. The predicted c_p values vary as well, showing noticeable deviation and disagreement between hypothermal and hyperthermal models at low s values. On the other hand, Sentman's model considers molecules random thermal motion, but it is built on the assumption of complete diffuse reflection. These models will not be discussed in detail here, since a comprehensive review can be found in [9, 27]. However, their fundamental assumptions are summarised in Fig. 1 and 2.

2. Scattering-kernel theory based GSI models

Scattering-kernel models, as we will refer to them in this section, are kinetic models built on a statistical approach. Correlation between the incident and reflected distributions of the particles is achieved through a proper definition of the boundary conditions for the collisionless Boltzmann equation in the rarefied gas regime. The correct formulation of these is of fundamental importance since boundary conditions describe the mechanisms that rule the interaction between gas and solid particles. When boundary conditions are written within the frame of the scattering-kernel theory, the problem consists in finding the most suitable expression for the scattering kernel $K(\mathbf{x}, t, \boldsymbol{\xi_i} \rightarrow \boldsymbol{\xi_r})$ to reproduce the interaction phenomena occuring at the surface under the assumptions considered.

Since an accurate knowledge of the dynamics and the thermodynamics of the interaction is not achievable, a quantity $P(\boldsymbol{\xi_i} \rightarrow \boldsymbol{\xi_r}, \mathbf{x_i} \rightarrow \mathbf{x_r}, t_i \rightarrow t_r)$ can be introduced to describe the density of probability that a gas particle impacting on a point $\mathbf{x_i}$ located on the surface, at a certain time t_i with an incident velocity corresponding to $\boldsymbol{\xi_i}$ is reflected at a generally different location $\mathbf{x_r}$ at time t_r with a velocity $\boldsymbol{\xi_r} \neq \boldsymbol{\xi_i}$ [62]. Assuming that the sitting time on the surface is low enough $(t_i \simeq t_r = t \rightarrow \mathbf{x_i} \simeq \mathbf{x_r} = \mathbf{x})$ such that no adsorption/desorption or diffusion phenomena need to be addressed [62]:

$$P(\boldsymbol{\xi_i} \rightarrow \boldsymbol{\xi_r}, \mathbf{x_i} \rightarrow \mathbf{x_r}, t_i \rightarrow t_r) = K(\boldsymbol{\xi_i} \rightarrow \boldsymbol{\xi_r}) \tag{19}$$

where the incident and reflected molecular velocity vectors more generally consist of two tangential ($[\xi_{i,t'}, \xi_{i,t''}]$, $[\xi_{r,t'}, \xi_{r,t''}]$) and one normal ($\xi_{i,n} < 0$, $\xi_{r,n} > 0$) component. Proposed classes of $K(\boldsymbol{\xi_i} \rightarrow \boldsymbol{\xi_r})$ not only need to correctly capture the phenomena occuring in the proximity of the wall through a proper correlation of the incident ($f_i(\boldsymbol{\xi_i})$) and reflected ($f_r(\boldsymbol{\xi_r})$) velocity distributions:

$$\xi_{r,n} f_r(\boldsymbol{\xi_r}) = \int_{\xi_{i,n}<0} K(\boldsymbol{\xi_i} \rightarrow \boldsymbol{\xi_r}) |\xi_{i,n}| f_i(\boldsymbol{\xi_i}) d\boldsymbol{\xi_i} \tag{20}$$

but also need to satisfy some specific conditions. The non-negativity condition [63]:

11

$$K\left(\boldsymbol{\xi_i} \rightarrow \boldsymbol{\xi_r}\right) \geq 0 \tag{21}$$

derives by the correlation existing between kernels and probabilty density functions. These last, being the derivative of the distribution function, are always non-negative in $\mathbb{R}$. The normalisation condition [63]:

$$\int_{\xi_{r,n}} K\left(\boldsymbol{\xi_i} \rightarrow \boldsymbol{\xi_r}\right) d\boldsymbol{\xi_r} = 1 \tag{22}$$

results from imposing balance between the mass flow arriving at the surface and the mass flow leaving the surface (see Eq. 20). From a physical point of view, normalising the scattering kernels is equivalent to stating that the particles involved in the interaction leave the boundary, so that no capture occurs. Finally, the reciprocity or detailed balance condition [63]:

$$f_0\left(\boldsymbol{\xi_i}\right)|\xi_{i,n}|K\left(\boldsymbol{\xi_i} \rightarrow \boldsymbol{\xi_r}\right) = f_0\left(\boldsymbol{\xi_r}\right)|\xi_{r,n}|K\left(-\boldsymbol{\xi_r} \rightarrow -\boldsymbol{\xi_i}\right) \tag{23}$$

is a balance equation according to which, for a gas-surface system in thermodynamic equilibrium, a correspondence can be established between 1) the scattering path of the particles and 2) the path that those particles would hypothetically follow if they travelled with velocities that are opposite to those considered in the same time interval [64]. This constraint stems by writing the boundary condition as a function of the temperature of the wall. In Eq. 23, f_0 indicates the Maxwellian velocity distribution function corresponding to T_w.

2.1. The Maxwell Model

In Maxwell's model [65] the behaviour of the reflecting surface is described by the linear combination of the two classical scattering characteristics mentioned in the previous paragraph. According to this, a fraction of incident particles, identifiable with the accommodation coefficient σ, is assumed to be trapped by a perfectly absorbing wall. After achieving complete accommodation, the particles are re-emitted from the surface with a Maxwellian velocity distribution typical of a gas at rest and in thermal equilibrium with the wall ($T_g = T_w$). The remaining fraction $(1 - \sigma)$ of the incident gas particles collides on an ideally smooth and elastic surface so that, after the collision, the momentum exchange occurs just along the normal direction and the reflected gas lies along the specular direction. The scattering kernel for this model is accordingly built as the sum of the scattering kernels for specular reflection and diffuse re-emission with complete thermal accommodation [66, 67]:

$$K_M(\boldsymbol{\xi_i} \rightarrow \boldsymbol{\xi_r}) = (1 - \sigma)\delta(\boldsymbol{\xi_i} - \boldsymbol{\xi_{r,specular}}) + \sigma f_0(\boldsymbol{\xi_r})|\xi_{r,n}| \tag{24}$$

where δ is the Dirac delta function. This isotropic scattering kernel satisfies the physical constraints discussed and, because of its simplicity, has found substantial success in DSMC implementations. According to the model however, scattering cosine distributions presenting peaks in proximity of the the specular direction (Figure 5) should be expected. As discussed in Section 4, experimental results show a more complex behaviour which is not predictable by the linear combination adopted by Maxwell, thus limiting the range of applicability of the model.
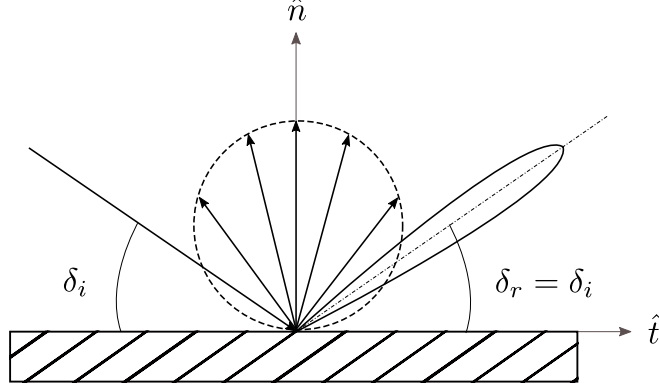
Figure 5: Schematic representation of the polar plot distribution predicted by the Maxwell model [56].

2.2. The Nocilla-Hurlbut-Sherman (NHS) Model

The NHS model, first proposed by Nocilla [68, 69] and refined by Hurlbut and Sherman [55] postulates a "drifting/shifted Maxwellian" law for the reflected particles distribution:

$$f_r(\boldsymbol{\xi}) = \frac{n_r}{(2\pi RT_r)^{3/2}} \exp\left[-\frac{(\boldsymbol{\xi} - \boldsymbol{v_r})^2}{2RT_r}\right] \tag{25}$$

where n_r is the scattering molecules density, T_r is the temperature associated with the scattered distribution, and $\boldsymbol{v_r}$ is the macroscopic or bulk velocity (drift) of the reflected particles. According to Equation 25, the reflected flux is described by v_r, the scattering angle $\delta_r = 90° - \theta_r$ determined by the direction of $\boldsymbol{v_r}$ with regards to the tangent to the surface, and T_r which in general can be different from T_s. In the original form proposed by Nocilla, the model contains the complementary cases of diffuse scattering ($v_r = 0$) and specular reflection ($s_r = s_i$, $\boldsymbol{v_r} = \boldsymbol{v_i}$, $\delta_r = \delta_i$). However, the mathematical formulation inherently suffers from the lack of connection between the incident and reflected velocity distributions. In this regard, Hurlbut and Sherman [55] introduced a drifting Maxwellian velocity distribution for the incident particles:

$$f_i(\boldsymbol{\xi}) = \frac{n_i}{(2\pi RT_i)^{3/2}} \exp\left[-\frac{(\boldsymbol{\xi} - \boldsymbol{v_i})^2}{2RT_i}\right] \tag{26}$$

and related the two distributions by determining n_r from the equivalence of the incoming and reflected number fluxes in stationary conditions. A model reformulation was also proposed to reduce the difficulties encountered in matching the experimental results with the model, which requires an accurate determination of T_r. A partial thermal accommodation coefficient $\alpha_{T,P}(\theta_i) \sim \alpha_{T,P}(\delta_i)$, avaraged over all the possible scattering directions and defined for a specific angle of incidence δ_i, was accordingly introduced [55]:

$$\alpha_{T,P}(\delta_i) = \frac{E_i(\delta_i) - E_r}{E_i(\delta_i) - E_w} \tag{27}$$

13

and analytic expressions for the computation of the aerodynamic drag and lift coefficients were determined. For a given angle of incidence of the flow, the aerodynamic coefficients are built as a function of v_r (or s_r), δ_r and $\alpha_{T,P}(\delta_i)$. Cercignani and Lampis [70] provided a reformulation of the NHS model in the context of the scattering kernel theory, following some suggestions already present in Nocilla's original proposal. Corrections to this model were also applied so that the proposed kernel could satisfy the normalisation (Eq. 22) and detailed balance conditions (Eq. 23) [71]. Despite these improvements and some early applications of the model for the computation of the aerodynamic coefficients in FMF conditions [72], further implementations did not find much success. However, the good agreement achieved with some gas-beam experimental results [55] for clean surfaces made the NHS model a fundamental starting point for advances in the study of gas-surface interaction.

2.3. The Cercignani-Lampis-Lord (CLL) Model

The Cercignani-Lampis [62] model (CL) is one of the most successful kernel-based representations of the gas particles-surface interaction as it is described by experimental results. The expression for the scattering kernel is obtained assuming no adsorption and independent interaction of each gas particle with the surface [62]:

$$
K_{CL}(\boldsymbol{\xi_i} \to \boldsymbol{\xi_r}) = \frac{1}{\alpha_n \sigma_t (2 - \sigma_t)} \exp\left[\frac{\alpha_n - 1}{\alpha_n} (\xi_{r,n}^2 + \xi_{i,n}^2) + \right.
$$
$$
- \frac{(1 - \sigma_t)^2}{\sigma_t (2 - \sigma_t)} (\xi_{r,t}^2 + \xi_{i,t}^2) +
$$
$$
\left. + \frac{2(1 - \sigma_t)}{\sigma_t (2 - \sigma_t)} (\boldsymbol{\xi_{i,t}} \cdot \boldsymbol{\xi_{r,t}}) \right] I_0\left[\frac{2(1 - \alpha_n)^{1/2}}{\alpha_n} \xi_{r,n} \xi_{i,n} \right]
\tag{28}
$$

where for both the incident and reflected velocity, $\xi_{j,t} = \sqrt{\xi_{j,t'}^2 + \xi_{j,t''}^2}$ and I_0 is the modified Bessel Function of the first kind and zeroth order. The density of probability described by Eq. 28 is given by the contributions coming from the variation of the three components of the velocity vector. Since the tangential and the normal components can be treated separately in the model, their individual scattering kernels can accordingly be derived. Following the formulation proposed by Lord [73] for isotropic surfaces, the scattering kernel for the normal component of velocity can be written:

$$
K_{CLL}(\xi_{i,n} \to \xi_{r,n}) = \frac{2\xi_{r,n}}{\alpha_n} I_0 \frac{2(1 - \alpha_n)^{1/2} \xi_{r,n} \xi_{i,n}}{\alpha_n} \times
$$
$$
\exp\left[-\frac{\xi_{r,n}^2 + (1 - \alpha_n)\xi_{i,n}^2}{\alpha_n} \right]
\tag{29}
$$

for which the reciprocity and normalisation conditions take the form:

$$
|\xi_{i,n}| \exp[-\xi_{i,n}^2] K_{CLL}(\xi_{i,n} \to \xi_{r,n}) = \xi_{r,n} \exp[-\xi_{r,n}^2] K_{CLL}(-\xi_{r,n} \to -\xi_{i,n})
\tag{30}
$$

$$
\int_0^\infty K_{CLL}(\xi_{i,n} \to \xi_{r,n}) d\xi_{r,n} = 1
\tag{31}
$$

14

The interaction phenomenon in the tangential directions is described by the same accommodation coefficient so that, following surface isotropy, the expressions of the scattering kernels for the two tangential components of velocity are in the form of:

$$K_{CLL}(\xi_{i,t} \to \xi_{r,t}) = \frac{1}{\sqrt{\pi \sigma_t(2 - \sigma_t)}} \times \exp\left\{-\frac{[\xi_{r,t} - (1 - \sigma_t)\xi_{i,t}]^2}{\sigma_t(2 - \sigma_t)}\right\} \tag{32}$$

which satisfies:

$$\exp[-\xi_{i,t}{}^2]K_{CLL}(\xi_{i,t} \to \xi_{r,t}) = \exp[-\xi_{r,t}{}^2]K_{CLL}(-\xi_{r,t} \to -\xi_{i,t}) \tag{33}$$

$$\int_{-\infty}^{\infty} K_{CLL}(\xi_{i,t} \to \xi_{r,t})d\xi_{r,t} = 1 \tag{34}$$

As the equations above suggest, the dynamic of the interaction is regulated by two adjustable parameters: the normal energy accommodation coefficient (α_n) and the tangential momentum accommodation coefficient (σ_t). Lord contributed significantly to the success of the CL model whilst adapting it for DSMC implementation [74] and further extended its validity to cases excluded by the original model, among which diffuse re-emission with incomplete accommodation [73, 75] . Because of this, it is generally preferred to refer to the model as the Cercignani-Lampis-Lord model (CLL).

A possible implementation of the CLL model in closed-form solutions was proposed by Walker et al. [45]. The authors suggested modified expressions of the Schaaf and Chambre [41, 43] (S&C) closed form equations with the CLL model. The attempt is rather difficult since, among other parameters (Fig. 1), the S&C closed-form solutions are written as a function of σ_n and σ_t. While an immediate relation can be found between the tangential momentum accommodation coefficient and the tangential energy accommodation coefficient (α_t):

$$\alpha_t = \sigma_t(2 - \sigma_t) \tag{35}$$

the same cannot really be said for α_n and σ_n. Approximate analytic $\sigma_n - \alpha_n$ relations, written as a function of four best-fit parameters, were found adopting a least squares error approach and sensitivity analysis. Ranges of variation were selected for some meaningful parameters about their nominal values. In this way the agreement between the $\sigma_n - \alpha_n$ relation and the expected C_D values could be evaluated for the nominal conditions and over the range of variation of the selected parameters. These last were identified with the bulk velocity of the particles, the free stream temperature, the surface temperature, the normal thermal accommodation coefficient and the tangential momentum accommodation coefficient. Good correlation between the computed C_D and the values provided by the CLL model implemented in DSMC Analysis Code was seen for the modified S&C closed-form solutions written as a function of the derived $\sigma_n - \alpha_n$ laws. However, the set of values to be chosen for the best-fit parameters is not constant but varies with the gas species considered, the type of body impinged and, in the case of lighter molecular species, the α_n range assumed. Values suggested by Walker et al. for representetive molecular species and body shapes could be found in the original paper from the authors [45]. Bigger uncertainties are found in the case of He and H for value of α_n close to unity.

3. Physical GSI Models

Physical GSI models take advantage of experimental results to describe how the thermal motion of the surface influences the scattering dynamics of the impinging gas-beam. These models are thus based on assumptions regarding the surface interaction potentials, the surface morphological structure and the surface elasticity/stiffness characteristics. Among the vast number of models present in literature, special attention will be devoted to the simple quasi one-dimensional Hard Cube model and its most successful expansions: the Soft Cube model and the Washboard model. Two and three-dimensional lattice models [76–79] will be neglected in this review. These last are generally characterised by a more complex implementation which leads to higher accuracy and also computational time; factors potentially limiting the range of applicability of these models for the context of this paper. Moreover, if the increase in complexity is justified in the frame of pure gas-surface interaction, the same might not be true for orbital aerodynamics engineering applications. The number and range of uncertainties affecting the problem of aerodynamic forces and torques estimation in VLEO is quite high. Because of this, the increased level of complexity is likely to be unjustifiable against the numerous sources of errors observed.

3.1. The Hard Cube Model (HC)

The Hard Cube Model, as proposed in its earlier form by Goodman [80], has found success with Logan's and Stickney's [81] formulation. Despite its inherent simplicity, resulting from the assumptions adopted in its development, the model is able to qualitatively reproduce the experimental lobal scattering typical of clean and polished surfaces. The model assumes the surface to be perfectly smooth and the gas particles and surface atoms involved in the interaction to be ideally elastic and rigid. The dynamics of the collision is simplified by assuming that each gas particle interacts solely with a surface atom represented as an isolated cube in the lattice, so that any impact of the surface structure on the scattering properties is neglected. During the collision, the gas particle and the surface atom interact as free particles so that a one-dimensional impulsive-repulsive potential, with no attractive well, can be conjectured. In this way, the impact of interaction times on the collision mechanism can be ignored with benefits in terms of simplicity and with only a partial loss of accuracy. The cubes comprising the surface are oriented so that one of their four faces lies in the direction parallel to the surface contour and they are characterised by an initial Maxwellian normal velocity distribution determined by the surface temperature. The momentum exchange is assumed to be due uniquely to the normal component of the gas particle velocity (v_n) as the tangential component (v_t) is preserved by the surface properties (Figure 6). The model predicts a quasi-specular re-emission both above and below the specular range with each scattering angle θ_r being determined by a unique value of $v_{r,n}$ for a given $v_{i,t} = v_{r,t}$.

Along with the numerical formulation, an analytical approach in which mean velocity values are adopted instead of velocity distributions for both the gas particles and the surface atoms was proposed by Logan and Stickney [81]. According to this approach, closed form solutions can be derived and the parameters on which the interaction depends can be more easily identified. The flat surface assumption allows the restriction of the analysis to the plane identified by the surface normal and the incident velocity vector, so that:

$$\theta_r = \cot^{-1}\left[\cot\left(\theta_i\right)\left(\frac{1-\mu}{1+\mu} + \frac{16\mu}{9\pi\left(1+\mu\right)}\frac{T_w}{T_g\cos^2\left(\theta_i\right)}\right)\right] \tag{36}$$

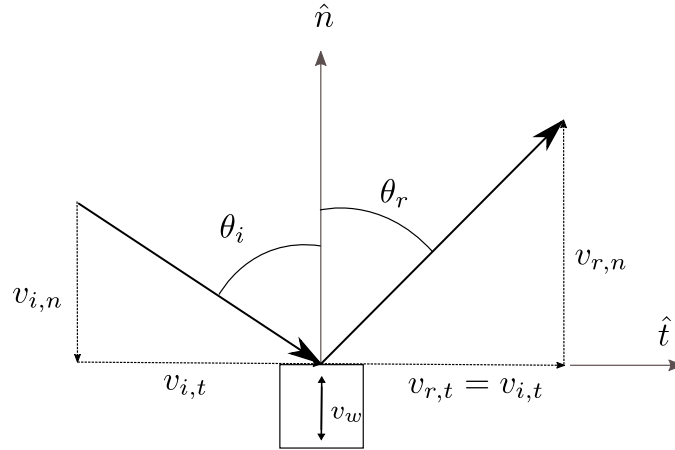where μ, the gas particle-surface atom mass ratio, is restricted to vary in the following range:

Figure 6: Hard Cube Model, reproduced from [81].

$$0 < \mu = \frac{m_g}{m_s} < \frac{1}{3} \tag{37}$$

and T_g is the gas-beam source temperature. Constraints on the possible values of μ result from further assuming that the gas particle experiences a single interaction with the surface atom considered. According to equation (36), the scattering direction depends on the mass ratio μ, the incidence angle and the surface-to-gas temperature ratio. Simplicity and ease in implementation are however obtained at the price of a general loss in accuracy in describing the experimental results compared to the extended model described in [81], for which numerical simulation is needed.

Some expansions of the HC model have been proposed, the most successful one discussed later in this section. Hurst et al. [82] and Nichols et al. [83, 84] modified the model to capture rotational dynamics of elliptically-shaped diatomic molecules scattered from the surface. Doll [85] addressed the rotational dynamics modelling diatomic homonuclear molecules as rigid rotors with motion restricted to a single plane. The importance for this model of multiple collisions with the surface atom arising from the rotational state were also discussed. Trapping phenomena were addressed by Weinberg and Merrill [86]. Trilling and Hurkmans [87] introduced an attractive long-range Coulomb potential, an exponential short-range repulsive potential and modified the surface geometry treating atoms as "spherical caps" rather then cubes. Sitz et al. [88] expanded the HC model to qualitatively describe momentum orientation in the scatterring of N_2 from smooth Ag(111), introducing a frictional force along the surface tangential direction. The additional level of complexity characterising these models seems inappropriate for the applications for which this review paper is intended and, because of this, they will not be discussed more thoroughly in the following sections.
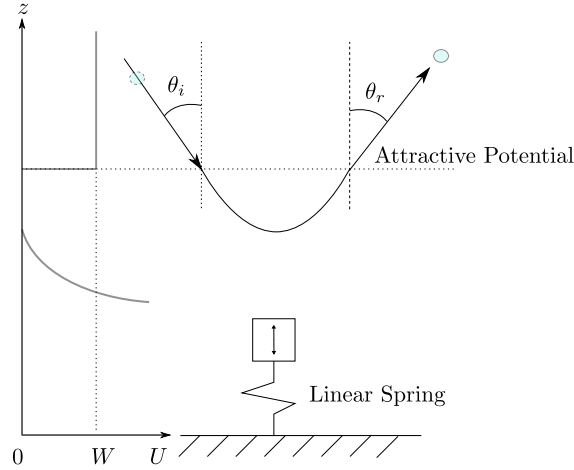
Figure 7: The Soft Cube Model, reproduced from [89].

3.2. The Soft Cube Model

The Soft Cube Model proposed by Logan and Keck in 1968 [89] owes its name to the introduction of a more realistic "soft" potential to capture the physics of the gas-surface interaction. The atoms that comprise the flat surface and take part in the collision are assumed to behave like independent cubes linked to the underlying lattice by means of single linear springs (Figure 7). Surface atoms are thus regarded as oscillators characterised by a natural frequency ω and a Maxwellian energy distribution corresponding to the surface temperature T_w. Similarly to the HC model, the interaction with a gas particle involves a single cube in the lattice and the energy exchange, responsible for the accommodation coefficient value, is due solely to the variation of the normal component of velocity after the collision ($v_{i,t} = v_{r,t}$). The interaction is however more realistically captured assuming non-negligible collision times, described by a non-impulsive interaction potential consisting of two components. In addition to a repulsive exponential potential, which substitutes the impulsive repulsive interaction assumed in the HC model, an attractive long-range square-well potential component is introduced. The model can be eventually employed to obtain an estimate of the fraction of particles that remain trapped on the surface after the collision and depart from it after achieving sufficient energy.

Comparison with experimental results is obtained by properly selecting the value of three modifiable parameters: 1) the potential well-depth W, 2) the interaction range b and 3) the oscillator frequency ω, whose value is assumed to be given by the Debye temperature (Θ_D). Combinations of b and W that reproduce, with satisfactory agreement, the experimental data referred to a selection of gas-surface systems can be found in the original paper by Logan and Keck [89].

3.3. The Washboard Model

Like the Soft Cube Model, the Washboard model [90] can be regarded as an attempt to improve the Hard Cube model agreement with the experimental results. Compared to the other GSI models discussed so far, the Washboard model has the advantage of addressing the effect of surface corrugation on the scattering properties while preserving relative clarity and simplicity.
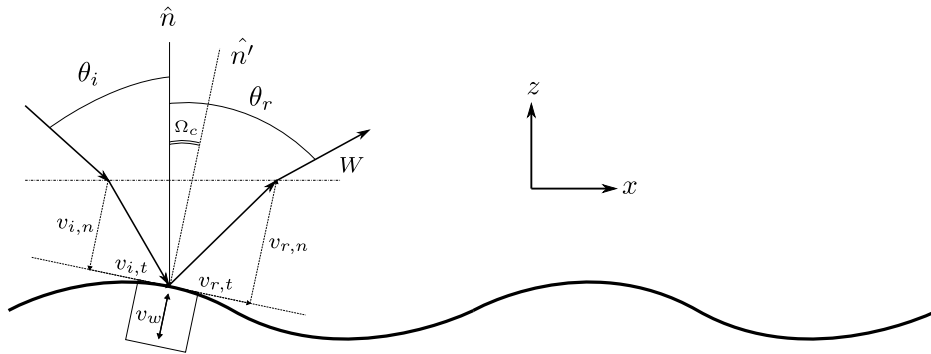
Figure 8: The washboard model, reproduced from [90].

The surface contour is simplified assuming a sinusoidal profile applied exclusively in one direction, thus making the model appropriate for bidimensional but not for out-of-plane scattering evaluation. Similarly to the HC model, the cube with which the colliding gas particle interacts is oriented along the surface contour and its velocity is determined by a Maxwellian distribution at the surface temperature. Because of the surface corrugation, the cubes are tilted with regards to the normal to the flat surface so that, for any impact point, a local normal and tangential directions can be identified (Figure 8). The maximum deviation of the local normal from the flat surface normal direction is measured by the corrugation strength parameter (Ω_C). The introduction of this parameter allows the model to adapt to different levels of surface corrugation, thus providing good qualitative agreement with experimental results ranging from smooth to rough surfaces. The attractive potential well W produces refraction in the gas particle initial trajectory, thus varying its normal and tangential component of velocity. Even in this case the nature of the interaction is impulsive so that in the local normal-tangential reference system, the tangential momentum is unchanged and the energy exchange is determined solely by the normal momentum variation. As a consequence, in the xz flat surface reference system the tangential momentum is not conserved and the strict assumption characterising both the Hard and the Soft Cube model is accordingly removed.

Analytic expressions for the angular scattering velocity and kinetic energy distributions were provided for small surface corrugations. The parameters on which these depend are the corrugation strength coefficient Ω_C, the incident angle θ_i, the incident kinetic energy E_i, the mass ratio μ, the potential well W and the surface temperature T_w. Eventually, the trapping probability can also be addressed. Further extensions of the washboard model include the works of Yan et al. [91] and Liang et al. [92].

4. Comparison of GSI Models with Gas-Beam Experiments

Molecular beam experiments are a useful means of gaining information concerning the energy exchange at the surface and the wall-gas system characteristics at atomic scale. For appropriate selection of incident energy distributions, the scattering of neutral molecules on a target

19

is representative of orbital conditions and can thus be used to investigate the aerodynamic behaviour of specific materials in the context of space applications. The literature covering the topic is vast and this section does not claim to be exhaustive, since such an activity would require a specific review effort. The objective is thus to provide an overall picture of the subject, focusing the attention on the physical regimes that are significant for the purpose of this paper, thus addressing, wherever possible, the points of strength and the limits of the models previously discussed in the context of VLEO aerodynamics. At VLEO altitudes, AO is the dominant constituent of the residual atmosphere, with atoms impacting on the exposed surfaces with an average velocity of $\sim$ 7.8 $km\ s^{-1}$ corresponding to a Maxwellian mean incident energy distribution of $\sim$ 5 eV. According to this, attention will be devoted especially to results referring to molecular beam scattering of monoatomic species from targets in a variety of conditions. Studies analysing diatomic and polyatomic beams scattering are numerous but their results are typically more difficult to interpret: the interaction depends on both the translational and internal energies of the molecule considered and on the local aspect of the interaction potential. However, results for N_2 and O_2 scattering from Ag(111) reported by Asada et al. [93] show mean velocity and mean energy distributions with scattering angle which are similar to those obtained for monoatomic molecules. Similarly, analysis of adsorption and desorption rates, which are important especially for heavier molecular species, requires correlation between the characteristics of the system interaction potential and the sticking probability. These, in turn, vary with initial rotational and translational energies, binding energies, orientation of the molecules, incidence angle and surface temperature [94]. Because of this, the spatial distributions obtained are the result of a complex mechanism of interaction [95, 96] and more advanced numerical tecnhiques involving molecular dynamics or binary collision approximation are required. Extensive reviews on the topic are however available in [97–102] with some more dated results reported in [103].

The scattering behaviours observed are not constant as they tend to change substantially with the system considered and, in particular, with the ratio between the mass of the gas particles and the surface atoms, the range of interaction, the energy/temperature of the incident beam with regards to the surface temperature, the molecular or atomic species involved in the experiment, the presence of adsorbents on the target surface, the morphology of the surface considered despite the level of roughness and the relative position and orientation of the gas particles and surface atoms [97]. At the time of writing, a comprehensive theory capable of capturing each possible scenario is not available such that multiple models, suitable for specific physical regimes, are adopted instead. For light particles and low incidence energies [98] compared to solid maximum phonon energy, the interaction is predominatly elastic. In these conditions, no energy transfer occurs in the system and quantum mechanical phenomena, such as diffraction, are expected to be predominant [97].

As gas particles mass and incident energy increases, the collisions become more inelastic in nature and classic theory is adequate enough to reproduce the scattering behaviour. For this physical range, whether particles gain or transfer energy to the surface depends on the relative magnitude of E_i and T_w. Generally three mechanisms of interaction are identified: 1) Single gas-surface collision with moderate net energy exchange; 2) Multiple gas-surface collisions with no adsorption and delayed scattering; 3) Multiple gas-surface collisions with adsorption to the surface and eventual desorption in the scattered gas. The latter interaction mode is typical of highly contaminated surfaces [104–106]: in these conditions, the adsorbed particles have time to reach equilibrium with the surface and they are scattered according to a cosine distribution with θ_r and a Maxwellian translational velocity distribution corresponding to the wall temperature. The majority of works published in literature, however, refer to the first two interaction scenarios,

20

typically observed in scattering from clean flat surfaces in Ultra High Vacuum (UHV) conditions. In this case, lobal re-emission distributions characterised by a predominant asymmetrical quasi-specular component are observed for varying surface properties, incident particles energies and wall temperature [93, 106–110, 110, 111]. The generally small amount of particles that undergo multiple collisions before being scattered in the gas-phase determines the width of the lobe of distribution and seems to be susceptible to the morphology of the surface considered, despite the level of roughness. Wider angular distributions were obtained for smoother surfaces even when higher incident energies were employed [107]. This seems to suggest that the interactions within atoms in the same surface layer or adjacent layers may play a role in determining the scattering characteristic.

In the inelastic scattering domain, however, different scattering behaviours and thus different trends are expected according to the incident energy and the interaction radius for the system considered [112]. As highlighted by Goodman in [97], for gas-surface systems that are not characterised by a strong periodicity in the interaction potential, low values of incident kinetic energy ($E_i < k_B T_w$) and large interaction distances [1] define the so-called *thermal scattering* regime. In these conditions, the impinging gas-particles can not see the surface corrugation and the surface appears flat and smooth. During the interaction, the tangential component of momentum is generally conserved and the scattering dynamics are dominated by the surface thermal motion in the direction normal to the surface. Thermal scattering studies [106, 109, 113–116] show the following common features for the angular distributions (Fig. 9):

1. $\partial\theta_{r,max}/\partial T_w \leq 0$: the scattering angle corresponding to the peak in the distribution slightly moves towards the normal to the surface with increasing T_w [117]. Moreover, at high values of T_w, for which the surface appears to be free of adsorbents, the width of the distribution experiences a slight increase with decreasing T_i/T_w [106, 113]. Higher T_w also induces lower scattering intensity at the peak of the distribution [113, 116]. Some authors, however, obtained the opposite trend for the scattering of Ar [118], Xe [116, 118] and Kr [113, 118] on various metal surfaces at $T_i = T_{amb}$. Generally speaking, high wall temperatures are efficient in reducing the sticking probability and the time required for the interaction, thus preventing complete accommodation;

2. $\partial\theta_{r,max}/\partial\theta_i \geq 0$: the scattering angle corresponding to the peak in the distribution moves towards the surface tangent as the incidence angle increases [81, 106, 114, 115]. Moreover, $\partial\theta_{r,max}/\partial m_g \leq 0$, i.e. the scattering angle for which the distribution presents a peak moves towards the normal to the surface as the mass of the incident gas atom increases [81, 106, 119];

As the incident kinetic energy of the beam increases (within the limits of the thermal scattering domain), the effect of surface thermal vibration on the angular scattering distribution becomes less dominant. As a consequence, the lobal distribution becomes narrower and more symmetrical in shape, the scattered intensity at the peak increases [113] and $\theta_{r,max}$ generally moves towards the tangent to the surface [108, 112, 119, 120] (Figure 10, top right). When this condition is observed, the re-emission distribution is said to be *superspecular*. The effect seems to be more

---

[1]The interaction distance is defined here following the definition of the non-dimensional radius parameter R provided by Goodman in [97]. The distance of interaction is thus defined as the ratio between two quantities: the closest distance that separates the centre of the impinging atom from the centre of the surface atom during the collision and the critical value of this distance for the gas-surface system considered. When the critical distance value is achieved the impinging particle enters the surface.
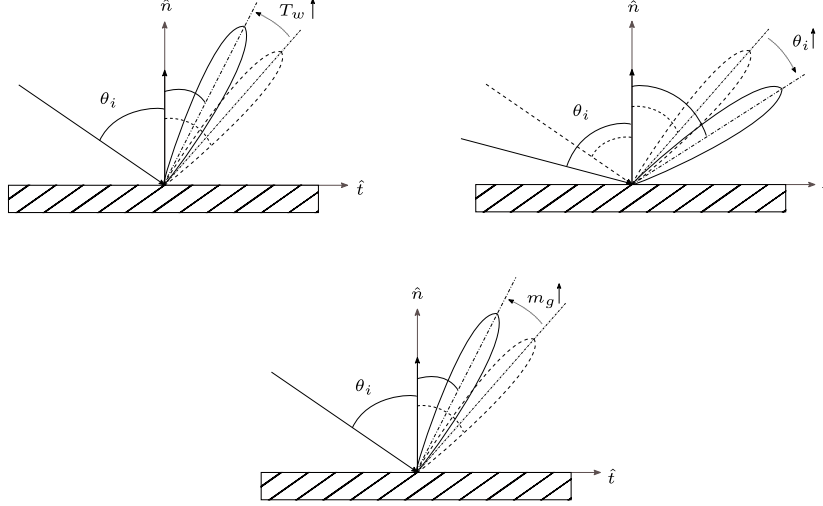
Figure 9: Variation of $\theta_{r,max}$ - the angle at which the peak of the distribution occurs - in the thermal scattering regime. Behaviours observed with increasing T_w (top left), θ_i (top right) and m_g (bottom) are illustrated.

noticeable for nearly grazing angles of incidence [108]. With regards to translational energy distributions, when the conservation of the tangential momentum is observed, the relative ratio between the mean final and incident energies varies according to the parallel momentum conservation curve:

$$\frac{E_r}{E_i} = \frac{\sin^2 \theta_i}{\sin^2 \theta_r} \tag{38}$$

The characteristics mentioned above are well described by the cube models [117] reviewed in the previous section of this paper, because of the inherent assumptions on which these models are built. Better agreement, as expected, is found with the SC [89, 105, 106] rather than with the HC model [108, 112, 113, 116, 117, 121], not only because of the more realistic gas-surface interaction potential assumed, but also because adjustments can be made through the parameter W for the system considered. When the attractive well W dominates the dynamics, the repulsive potential assumption loses accuracy and the HC model fails in describing trapping and partial accommodation to the surface. The limitations imposed on the gas particle-surface atom mass ratio in the HC model are likely to make the model unsuitable for addressing atomic oxygen scattering from most surfaces. Moreover, comparison of the potentialities of these two models against experimental data is possible just in the incident scattering plane. For out of plane scattering considerations, techniques addressing surface corrugation in more than one dimension need to be employed. While Maxwell's model fails in reproducing the petal-shaped angular distribution observed in these experiments, it appears that its theoretical apparatus and simplified assumptions are sufficient to describe some re-emission polar plots showing a small nearly specular and a large diffuse component [104, 107]. Results provided by Mehta et al. [108] show that when the CLL model is adopted some difficulties are encountered in the attempt of selecting the
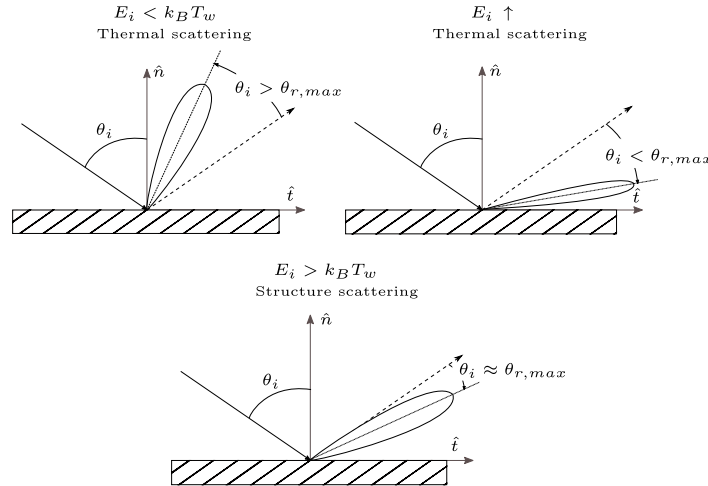
Figure 10: Transition from thermal to structure scattering with increasing values of E_i.

proper combination of α_n and σ_t to reproduce the experimental conditions. Excellent predictions of the position of the peak ($\theta_{r,max}$) and of the dispersion of the scattering distribution, for selected values of the accommodation coefficients, seem to exclude an accurate representation of the experimental E_r/E_i, and viceversa.

As the kinetic incident energy of the beam increases [117, 122, 123] with regards to the surface atoms thermal energy ($E_i > k_B T_w$) and the radius of interaction reduces, transition to the *structure scattering regime* is experienced: in this case, the surface roughness sensed by the impinging particles is noticeable because of the increased power of penetration. The interaction is no longer dominated by the surface thermal motion but by the surface corrugation. Because of the multiple collisions experienced by the particles with the rough surface, the angular distribution in this regime becomes wider in shape, the value of the peak scattered intensity decreases and a shift from superspecular to directions closer to the specular range for $\theta_{r,max}$ is observed [115, 124]. The qualitative re-emission behaviour expected for increasing value of E_i in the transition from the thermal to the structure regime are reproduced in Figure 10. In contrast to the thermal regime, the energy of the scattered beam (E_r) increases with increasing θ_r [117, 125]. Cube models relying on the flat surface approximation, are unable to reproduce this scenario and agreement is rather found with the Hard Spheres model [126], the Washboard model [120], and, in general, more complex models. Accordance of the HC model with some gas-beam data referred to hyperthermal E_i seems fortuitous [127] and, according to the authors, attributable to the morphology of the gas-surface system considered. An interesting scattering phenomenon observed in the structure regime is rainbow scattering: when this process occurs the typically wide spatial distribution is characterised by two peak lobes corresponding to different intensities in the flux measurements. This phenomenon was however, predominantly observed on the scattering of rare gases from LiF surfaces [128, 129], with some evidence on systems composed by metal surfaces [120, 130]. More details on the topic can be found in [97, 98]. The appearance of rainbow scattering effects seems to be associated with surface corrugation. In this regard, the Washboard model offers a relatively simple formulation able of capturing more complicated re-

emission mechanisms for which the HC and SC models are not suited. Moreover, the Washboard model appears to be more effective in describing gas particle attraction and surface penetration as well as scattering characteristic from softer surfaces [121], especially if compared with the HC model. These features are particularly useful when studying gas-surface interaction specifically for orbital aerodynamic applications. The interaction of most materials with the orbital environment is likely to cause variations in the static gas-surface potential corrugation [57] and, more in general, degradation of material performances with time. The lattice structure is subjected to become rougher as AO exerts its erosion action on the ram surfaces. As a consequence, materials with promising aerodynamic performances (i.e. near-specular re-emissions) might experience variations in the expected scattering behaviour within a mission lifetime. In this scenario, the principles on which the Washboard model is built could prove useful to address materials degradation and performance variation.

5. Conclusions

Renewed interest in small satellites missions in the lower region of the Earth's atmosphere demands new aerodynamic technologies capable of taking advantage of the environment in LEO. Aerodynamic performances are dependent on the mechanisms that rule the gas-solid interaction, but great uncertainties are associated with the physical processes occurring at the wall in rarefied and extremely rarefied regimes. Gas-beam experimental results suggest that reality might be more complex than that described by classical theoretical kinetic models. The development of a new generation of aerodynamic materials may therefore require more accurate predictions. The number of uncertainties in the system behaviour reflects a vast production of models in literature: difficulties however arise in the attempt of combining efficiency with simplicity. In the previous sections popular models which have obtained considerable success for their immediacy and ability to predict scattering behaviours have been reviewed. These models were broadly associated with two principal families according to some common features. Scattering-kernel theory based GSI models are built on a statistical approach, while physical GSI models provide a simple tools to describe the complex physical interaction mechanisms observed at the wall. Wherever possible, their appropriateness has been discussed against relevant gas-beam experimental results for the problem considered and physical ranges of application have been identified.

The joined effort of several authors has resulted in remarkable improvements in the understanding of the phenomena involved in the observed re-emissions. The problem is however complex and multidisciplinary in nature. Despite the challenges that remain, they represent a starting point for future developments. At the moment of writing, it appears that an easy-to-implement model applicable to different scattering regimes and to different gas-solid systems is still to be defined. Similarly, a simple analytical model capable of a more accurate quantitative description of the behaviours of both clean and contaminated surfaces might be desirable. In this regard, the level of technological advancement achieved by gas-beam facilities seems adequate to support a more critical analysis of the models developed so far. A more scrupulous examination of the approximations on which these rely may help in identifying the points of strength of each model and possibly expand their range of applicability. There might also be a chance to identify with more accuracy the re-emission patterns that an improved GSI model should be able to describe. A possible strategy may include enriching the proposed scattering-kernels for GSI with some more realistical assumptions regarding adsorption and desorption phenomena. Further comparison of theoretical models addressing surface corrugation with a broader range of experimental data might be helpful as well. Due to the wide amount of results concerning

24

scattering from clean surfaces, the majority of works seem to focus mainly on comparison with the simpler HC and SC models. The Washboard model appears to be privileged in the study of rainbow scattering from extremely corrugated surfaces. However, using this model against data referring to less corrugated surfaces might facilitate the understanding of the GSI problem.

Some adaptability characteristics are especially desired when VLEO aerodynamic applications are discussed. The growing interest in Earth-observation missions at these altitudes has paved the way for the study of aerodynamic materials promoting nearly specular reflection. However, the results obtained in a controlled facility may be affected by considerable alterations in the real thermospheric environment. A robust GSI model capable of providing satisfactory agreement for a range of interaction performance can facilitate the task of designing aerodynamic features for VLEO satellites. As a consequence, increase in the reliability of the aerodynamic control manoeuvres proposed in literature is expected. End-of-life tasks, satellite geometry and ABEP system design are likely to benefit from any knowledge improvement as well. This task, although difficult, seems to be easier to achieve in the context of orbital aerodynamics. The requirements imposed on the accuracy of the model are more relaxed than those expected in the more general frame of gas-surface interaction science. This is a result of the considerable number of additional uncertainties that affect the estimation of the aerodynamic forces and torques. A less accurate but still effective model may therefore adequately serve the purpose of describing a range of scattering behaviour or, equivalently, aerodynamic performance.

6. Acknowledgements

References

[1] R. Lyle, P. Stabekis, L. Sentman, R. Passamaneck, Spacecraft Aerodynamic Torques, Technical Report January, NASA Space Vehicle Design Criteria (Guidance and Control), 1971.

[2] E. Doornbos, H. Klinkrad, Modelling of space weather effects on satellite drag, Advances in Space Research 37 (2006) 1229–1239. doi:10.1016/j.asr.2005.04.097.

[3] F. A. Marcos, W. J. Burke, S. T. Lai, Thermospheric Space Weather Modeling, in: 38th AIAA Plasmadynamics and Lasers Conference, Miami, FL, 2007. doi:10.2514/6.2007-4527.

[4] D. J. Gorney, Solar Cycle Effects on the Near-Earth Space Environment, 1990. doi:10.1029/RG028i003p00315.

[5] A. E. Hedin, H. G. Mayr, Solar EUV induced variations in the thermosphere, Journal of Geophysical Research 92 (1987) 869. URL: http://doi.wiley.com/10.1029/JD092iD01p00869. doi:10.1029/JD092iD01p00869.

[6] A. D. Danilov, J. Lastovička, Effects of geomagnetic storms on the ionosphere and atmosphere, International Journal of Geomagnetism and Aeronomy 2 (2001) 209–224. URL: http://elpub.wdcb.ru/journals/ijga/v02/gai99312/gai99312.pdf.

[7] R. D. Hunsucker, Atmospheric Gravity Waves Generated in the High-Latitude Ionosphere: A review, Reviews of Geophysics and Space Physics 20 (1982) 293–315. doi:10.1029/RG020i002p00293.

[8] A. D. Richmond, Gravity Wave Generation, Propagation, and Dissipation in the Thermosphere, Journal of Geophysical Research 83 (1978) 4131. doi:10.1029/JA083iA09p04131.

[9] D. Mostaza Prieto, B. P. Graziano, P. C. Roberts, Spacecraft drag modelling, Progress in Aerospace Sciences 64 (2014) 56–65. URL: http://dx.doi.org/10.1016/j.paerosci.2013.09.001. doi:10.1016/j.paerosci.2013.09.001.

[10] P. Roberts, N. Crisp, S. Edmondson, S. Haigh, R. Lyons, V. Oiko, A. Rojas, K. Smith, J. Becedas, G. González, I. Vázquez, Á. Braña, K. Antonini, K. Bay, L. Ghizoni, V. Jungnell, J. Morsbøl, T. Binder, A. Boxberger, G. Herdrich, F. Romano, S. Fasoulas, D. Garcia-Almiñana, S. Rodriguez-Donaire, D. Kataria, M. Davidson, R. Outlaw,

B. Belkouchi, A. Conte, J. Perez, R. Villain, B. Heißerer, A. Schwalber, Discoverer - Radical redesign of earth observation satellites for sustained operation at significantly lower altitudes, in: Proceedings of the International Astronautical Congress, IAC, volume 14, 2017, pp. 25–29. doi:`IAC-17-D1`.

[11] N. H. Crisp, P. C. Roberts, S. Livadiotti, V. T. Oiko, S. Edmondson, S. J. Haigh, C. Huyton, L. A. Sinpetru, K. L. Smith, S. D. Worrall, J. Becedas, V. Hanessian, J. Nielsen, M. Bisgaard, Y.-A. Chan, S. Fasoulas, G. H. Herdrich, F. Romano, C. Traub, D. Garcia-Almiñana, S. Rodriguez-Donaire, M. Sureda, D. Kataria, R. Outlaw, B. Belkouchi, A. Conte, J. S. Perez, R. Villain, B. Heißerer, A. Schwalber, The Benefits of Very Low Earth Orbit for Earth Observation Missions, Progress in Aerospace Sciences (2020).

[12] R. Bevilacqua, M. Romano, Rendezvous Maneuvers of Multiple Spacecraft Using Differential Drag Under J2 Perturbation, Journal of Guidance, Control, and Dynamics 31 (2008) 1595–1607. URL: `http://arc.aiaa.org/doi/10.2514/1.36362`. doi:`10.2514/1.36362`.

[13] D. Pérez, R. Bevilacqua, Differential drag spacecraft rendezvous using an Adaptive Lyapunov Control strategy, Advances in the Astronautical Sciences 145 (2012) 973–991. doi:`10.1016/j.actaastro.2012.09.005`.

[14] L. Dell' Elce, G. Kerschen, Optimal propellantless rendez-vous using differential drag, Acta Astronautica 109 (2015) 112–123. URL: `http://dx.doi.org/10.1016/j.actaastro.2015.01.011`. doi:`10.1016/j.actaastro.2015.01.011`.

[15] J. Virgili Llop, P. C. Roberts, K. Palmer, S. Hobbs, J. Kingston, Descending Sun-Synchronous Orbits with Aerodynamic Inclination Correction, Journal of Guidance, Control, and Dynamics 38 (2015) 831–842. URL: `http://arc.aiaa.org/doi/10.2514/1.G000183`. doi:`10.2514/1.G000183`.

[16] J. Virgili-Llop, P. C. E. Roberts, N. C. Hara, Atmospheric Interface Reentry Point Targeting Using Aerodynamic Drag Control, Journal of Guidance, Control, and Dynamics 38 (2015) 403–413. URL: `http://arc.aiaa.org/doi/10.2514/1.G000884`. doi:`10.2514/1.G000884`.

[17] H. Leppinen, Deploying a single-launch nanosatellite constellation to several orbital planes using drag maneuvers, Acta Astronautica 121 (2015) 23–28. URL: `http://dx.doi.org/10.1016/j.actaastro.2015.12.036`. doi:`10.1016/j.actaastro.2015.12.036`.

[18] S. Omar, R. Bevilacqua, Guidance, navigation, and control solutions for spacecraft re-entry point targeting using aerodynamic drag, Acta Astronautica 155 (2019) 389–405. URL: `https://linkinghub.elsevier.com/retrieve/pii/S0094576518302893`. doi:`10.1016/j.actaastro.2018.10.016`.

[19] K. C. Pande, R. Venkatachalam, On optimal aerodynamic attitude control of spacecraft, Acta Astronautica 6 (1979) 1351–1359. doi:`10.1016/0094-5765(79)90127-9`.

[20] T. H. Stengle, MagSat Attitude Dynamics and Control: Some Observations and Explanations, in: Fiifth Annual Flight Mechanics/Estimation Theory Symposium, 1980.

[21] M. L. Gargasz, Optimal Spacecraft Attitude Control Using Aerodynamic Torques, Ph.D. thesis, Air Force Institute of Technology, 2007.

[22] J. Auret, W. H. Steyn, Design of an aerodynamic attitude control system for a CubeSat, 62nd International Astronautical Congress 2011, IAC 2011 11 (2011) 9009–9017.

[23] J. Virgili, P. C. Roberts, ∆Dsat, a QB50 CubeSat mission to study rarefied-gas drag modelling, Acta Astronautica 89 (2013) 130–138. URL: `http://dx.doi.org/10.1016/j.actaastro.2013.04.006`. doi:`10.1016/j.actaastro.2013.04.006`.

[24] J. Virgili-Llop, P. C. Roberts, Z. Hao, Aerodynamic attitude and orbit control capabilities of the ∆DSAT cubesat, Advances in the Astronautical Sciences 151 (2014) 321–332.

[25] Z. Hao, P. C. Roberts, Using Aerodynamic Torques To Aid Detumbling Into an Aerostable State, 67th International Astronautical Congress (2016) 26–30.

[26] D. Mostaza-Prieto, P. C. Roberts, Perigee Attitude Maneuvers of Geostationary Satellites During Electric Orbit Raising, Journal of Guidance, Control, and Dynamics 40 (2017) 1978–1989. doi:`10.2514/1.G002370`.

[27] D. Mostaza-Prieto, Characterisation and Applications of Aerodynamic Torques on Satellites, Ph.D. thesis, University of Manchester, 2017.

[28] V. Cañas, E. Deimos, J. Becedas, R. M. Dominguez, P. C. E. Roberts, Attitude control for satellites flying in VLEO using aerodynamic surfaces, in: Reinventing Space Conference 2018, November, 2018. URL: `https://www.researchgate.net/publication/338573033`.

[29] G. B. Palmerini, S. Sgubini, G. Taini, Spacecraft orbit control using air drag, in: International Astronautical Conference, January 2005, 2014.

[30] C. Lambert, B. S. Kumar, J. F. Hamel, A. Ng, Implementation and performance of formation flying using differential drag, Acta Astronautica 71 (2012) 68–82. doi:`10.1016/j.actaastro.2011.08.013`.

[31] X. Shao, M. Song, J. Wang, D. Zhang, J. Chen, Satellite formation keeping using differential lift and drag under J2 perturbation, Aircraft Engineering and Aerospace Technology 89 (2017) 11–19. doi:`10.1108/AEAT-06-2015-0168`.

[32] D. Spiller, F. Curti, C. Circi, Minimum-Time Reconfiguration Maneuvers of Satellite Formations Using Perturbation Forces, Journal of Guidance, Control, and Dynamics 40 (2017) 1130–1143. URL: `https://arc.aiaa.`

org/doi/10.2514/1.G002382. doi:10.2514/1.G002382.

[33] R. Sun, J. Wang, D. Zhang, Q. Jia, X. Shao, Roto-Translational Spacecraft Formation Control Using Aerodynamic Forces, Journal of Guidance, Control, and Dynamics 40 (2017) 2556–2568. URL: https://arc.aiaa.org/doi/10.2514/1.G003130. doi:10.2514/1.G003130.

[34] M. Horsley, S. Nikolaev, A. Pertica, Small Satellite Rendezvous Using Differential Lift and Drag, Journal of Guidance, Control, and Dynamics 36 (2013) 445–453. URL: http://arc.aiaa.org/doi/10.2514/1.57327. doi:10.2514/1.57327.

[35] B. Smith, R. Boyce, L. Brown, M. Garratt, Investigation into the Practicability of Differential Lift-Based Spacecraft Rendezvous, 2017. URL: https://arc.aiaa.org/doi/10.2514/1.G002537. doi:10.2514/1.G002537.

[36] F. Romano, T. Binder, G. Herdrich, S. Fasoulas, T. Schönherr, Air-Intake Design Investigation for an Air-Breathing Electric Propulsion System, International Electric Propulsion Conference (2015) 1–27.

[37] J. Virgili Llop, P. C. Roberts, Z. Hao, L. Ramio Tomas, V. Beauplet, Very Low Earth Orbit mission concepts for Earth Observation. Benefits and challenges, in: Reinventing Space Conference 2014, January 2015, 2014, pp. 1 – 18.

[38] J. Virgili Llop, Spacecraft Flight in the Atmosphere (2014). doi:10.13140/RG.2.1.5192.8480.

[39] E. K. Sutton, Normalized Force Coefficients for Satellites with Elongated Shapes, Journal of Spacecraft and Rockets 46 (2009) 112–116. URL: http://arc.aiaa.org/doi/10.2514/1.40940. doi:10.2514/1.40940.

[40] L. H. Sentman, Free molecule flow theory and its application to the determination of aerodynamic forces, Technical Report, Lockheed Aircraft Corporation, Sunnyvale, California, 1961.

[41] J. A. Storch, Aerodynamic Disturbances on Spacecraft in Free-Molecular Flow, Technical Report, Los Angeles Air Force Base, CA 90245, 2002.

[42] G. A. Bird, Molecular Dynamics and the Direct Simulation of Gas Flows.pdf, Oxford, 1994.

[43] S. A. Schaaf, P. L. Chambre, Flow of Rarefied Gases, Princeton university Press, 1958. URL: https://www.jstor.org/stable/j.cttm32248.4.

[44] I. N. Ivchenko, S. K. Loyalka, R. V. J. Tompson, Analytical Methods for Problems of Molecular Transport, Springer, 2007.

[45] A. Walker, P. Mehta, J. Koller, Drag Coefficient Model Using the Cercignani– Lampis–Lord Gas–Surface Interaction Model, Journal of Spacecraft and Rockets 51 (2014) 1544–1563. URL: http://arc.aiaa.org/doi/10.2514/1.A32677. doi:10.2514/1.A32677.

[46] L. G. Jacchia, Thermospheric Temperature, Density, and Composition: New Models, SAO Special Report (1977). URL: http://adsbit.harvard.edu//full/1977SAOSR.375.....J/0000002.000.html.

[47] A. E. Hedin, H. G. Mayr, Solar EUV Induced Variations in the Thermosphere, Journal of Geophysical Research 92 (1987) 869–875.

[48] J. D. Fuller, R. H. Tolson, Improved Method for the Estimation of Spacecraft Free-Molecular Aerodynamic Properties, Journal of Spacecraft and Rockets 46 (2009) 938–948. URL: http://arc.aiaa.org/doi/10.2514/1.43205. doi:10.2514/1.43205.

[49] K. A. Hart, K. R. Simonis, B. A. Steinfeldt, R. D. Braun, Analytical Aerodynamic Force and Moment Coefficients of Axisymmetric Objects in Rarefied Flow, in: AIAA Atmospheric Flight Mechanics Conference, 2015, pp. 1–14. doi:10.2514/6.2015-0520.

[50] K. A. Hart, S. Dutta, K. R. Simonis, B. A. Steinfeldt, R. D. Braun, Analytically-derived Aerodynamic Force and Moment (2014) 1–14.

[51] E. M. Gaposchkin, Calculation of Satellite Drag Coefficient, Technical Report 8000, 1994.

[52] X. Jin, F. Huang, P. Hu, X. Cheng, Fast and accurate prediction for aerodynamic forces and moments acting on satellites flying in low-earth orbit, AIP Conference Proceedings 1786 (2016). doi:10.1063/1.4967690.

[53] P. M. Mehta, A. Walker, C. A. McLaughlin, J. Koller, Comparing Physical Drag Coefficients Computed Using Different Gas-Surface Interaction Models, Journal of Spacecraft and Rockets 51 (2014) 873–883. URL: http://arc.aiaa.org/doi/10.2514/1.A32566. doi:10.2514/1.A32566.

[54] M. Knudsen, Die molekulare Warmeleitung der Gase und der Akkommodationskoeffizient, Annalen der Physik 4 (1911).

[55] F. C. Hurlbut, F. S. Sherman, Application of the Nocilla wall reflection model to free-molecule kinetic theory, Physics of Fluids 11 (1968) 486–496. doi:10.1063/1.1691943.

[56] J. C. Maxwell, The Scientific Papers of James Clerk Maxwell, volume II, Dover Publications, New York, 1890. doi:10.1017/CBO9780511710377.

[57] B. A. Banks, K. K. de Groh, S. K. Miller, Low Earth Orbital Atomic Oxygen Interactions With Materials, 2004. URL: http://hdl.handle.net/2060/20040087142. doi:10.1557/PROC-851-NN8.1.

[58] K. Moe, M. M. Moe, Gas-surface interactions and satellite drag coefficients, Planetary and Space Science 53 (2005) 793–801. doi:10.1016/j.pss.2005.03.005.

[59] R. Schamberg, A new analytic representation of surface interaction with hypothermal free molecular flow with

application to neutral-particle drag estimates of satellites, Technical Report, RAND, Reseacrh Memorandum, 1959.

[60] F. O. Goodman, A three-dimensional Hard Spheres theory of scattering of gas atoms from a solid surface, Technical Report, National Aeronautics and Space Administration, 1967.

[61] G. E. Cook, Satellite Drag Coefficients, Technical Report, Defense Documentation Center for Scientific and Technical Information, Cameron Station Alexandria, Virginia, 1966. doi:10.1002/nav.3800080206.

[62] C. Cercignani, M. Lampis, Kinetic models for gas-surface interactions, Transport Theory and Statistical Physics 1 (1971) 101–114. doi:10.1080/00411457108231440.

[63] C. Cercignani, Rarefied Gas Dynamics: From Basic Concepts to Actual Calculations, Cambridge University Press, Cambridge, UK, 2000.

[64] C. Cercignani, Mathematical Methods in Kinetic Theory, second edi ed., 1990.

[65] J. C. Maxwell, On Stresses in Rarified Gases Arising from Inequalities of Temperature, 1878. doi:https://doi.org/10.1098/rspl.1878.0052.

[66] J. F. Padilla, I. D. Boyd, Assessment of Gas-Surface Interaction Models for Computation of Rarefied Hypersonic Flow, Journal of Thermophysics and Heat Transfer 23 (2009) 96–105. doi:10.2514/1.36375.

[67] S. K. Dadzie, J. G. Méolens, Anisotropic scattering kernel generalized and modified Maxwell boundary conditions, Journal of Mathematical Physics 45 (2004) 1804–1819. doi:10.1016/j.buildenv.2006.10.027. arXiv:0812.0143v2.

[68] S. Nocilla, Sull'Interazione tra i Flussi di Molecole Libere e Superficie Rigide, in: C. Ferrari (Ed.), Dinamica dei gas rarefatti, Springer, Varenna, Italy, 1964, pp. 333–368. URL: http://dx.doi.org/10.1007/978-3-642-11024-5.

[69] S. Nocilla, Basic Concepts in the Surface Interaction of Free-Molecular Flows or Molecular Beams, Meccanica 2(1) (1967) 34–40.

[70] C. Cercignani, M. Lampis, A. Lentati, A new scattering kernel in kinetic theory of gases, Transport Theory and Statistical Physics 24 (1995) 1319–1336. doi:10.1080/00411459508206026.

[71] C. Cercignani, M. Lampis, New Scattering Kernel for Gas-Surface Interaction, AIAA Journal 35 (1997) 1000–1011. URL: https://doi.org/10.2514/2.209. doi:10.2514/3.13619.

[72] F. G. Collins, E. C. Knox, Parameters of Nocilla Gas/Surface Interaction Model from Measured Accommodation Coefficients, AIAA Journal 32 (1994) 765–773. doi:10.2514/3.12051.

[73] R. G. Lord, Some further extensions of the Cercignani-Lampis gas-surface interaction model, Physics of Fluids 7 (1995) 1159–1161. doi:10.1063/1.868557.

[74] R. G. Lord, Application of the Cercignani-Lampis Scattering Kernel to Direct Simulation Monte Carlo Calculations, in: Proceedings of the 17th International Symposium on Rarefied Gas Dynamics, Weinheim, Germany, 1991, pp. 1427–1433.

[75] R. G. Lord, Some extensions to the Cercignani-Lampis gas-surface scattering kernel, Physics of Fluids A 3 (1991) 706–710. doi:10.1063/1.858076.

[76] R. A. Oman, Numerical Experiments on Scattering of Noble Gases from Single-Crystal Silver, The Journal of Chemical Physics 48 (1968) 3919–3929. doi:10.1063/1.1669716.

[77] L. M. Raff, J. Lorenzen, B. C. McCoy, Theoretical Investigations of Gas-Solid Interaction Phenomena. I, The Journal of Chemical Physics 46 (1967) 4265–4274. doi:10.1063/1.1840536.

[78] J. Lorenzen, L. M. Raff, Theoretical Investigations of Gas–Solid Interaction Phenomena. II. Three-Dimensional Treatment, The Journal of Chemical Physics 49 (1968) 1165–1177. doi:10.1063/1.1670205.

[79] J. D. McClure, Atomic and Molecular Scattering from Solids. II. Comparison of Classical Scattering Models in Relation to Experiment, The Journal of Chemical Physics 51 (1969) 1687–1700. doi:10.1063/1.1672253.

[80] F. O. Goodman, On the theory of Accommodation Coefficients - IV. Simple Distribution Function Theory of Gas-Solid Interaction Systems, Phys. Chem. Solids 26 (1965) 85–105.

[81] R. M. Logan, R. E. Stickney, Simple classical model for the scattering of gas atoms from a solid surface, The Journal of Chemical Physics 44 (1966) 195–201. URL: https://doi.org/10.1063/1.1726446. doi:10.1063/1.1726446.

[82] J. E. Hurst, G. D. Kubiak, R. N. Zare, Statistical Averaging in Rotationally Inelastic Gas-Surface Scattering: the Role of Surface Atom Motion, Chemical Physics Letters 93 (1982) 235–239. doi:10.1016/0009-2614(82)80130-9.

[83] W. L. Nichols, J. H. Weare, Homonuclear diatomic scattering from solid surfaces: A hard cube model, The Journal of Chemical Physics 62 (1975) 3754. doi:10.1063/1.430973.

[84] W. L. Nichols, J. H. Weare, Heteronuclear diatomic scattering from solid surfaces: A hard-cube model, Journal of Chemical Physics 63 (1975) 379–383. doi:10.1063/1.431112.

[85] J. D. Doll, Simple classical model for the scattering of diatomic molecules from a solid surface, The Journal of Chemical Physics 59 (1973) 1038–1042. doi:10.1063/1.1680146.

[86] W. H. Weinberg, R. P. Merrill, A Simple Classical Model for Trapping in Gas–Surface Interactions, Journal of

Vacuum Science and Technology 8 (1971) 718–724. doi:10.1116/1.1315383.

[87] L. Trilling, A. Hurkmans, The scattering of ions from a clean solid surface in the 1 to 10 eV range, Surface Science 59 (1976) 361–372.

[88] G. O. Sitz, A. C. Kummel, R. N. Zare, J. C. Tully, Direct inelastic scattering of N2 from Ag(111). II. Orientation, The Journal of Chemical Physics 89 (1988) 2572–2582. doi:10.1063/1.455052.

[89] R. M. Logan, J. C. Keck, Classical theory for the interaction of gas atoms with solid surfaces, The Journal of Chemical Physics 49 (1968) 860–876. URL: https://doi.org/10.1063/1.1670153. doi:10.1063/1.1670153.

[90] J. C. Tully, Washboard model of gas-surface scattering, The Journal of Chemical Physics 92 (1990) 680–686. URL: https://doi.org/10.1063/1.458421. doi:10.1063/1.458421.

[91] T. Yan, W. L. Hase, J. C. Tully, A washboard with moment of inertia model of gas-surface scattering, Journal of Chemical Physics 120 (2004) 1031–1043. doi:10.1063/1.1628674.

[92] T. Liang, Q. Li, W. Ye, A physical-based gas–surface interaction model for rarefied gas flow simulation, Journal of Computational Physics 352 (2018) 105–122. doi:10.1016/j.jcp.2017.08.061.

[93] H. Asada, M. Toshiji, Speed Distribution of Monatomic, Diatomic and Polyatomic Molecular Beams Scattered by the (111) Plane of Silver, Japanese Journal of Applied Physics 21 (1982) 259–263. doi:10.1143/JJAP.21.259.

[94] C. W. Muhlhausen, L. R. Williams, J. C. Tully, Dynamics of Gas-Surface Interactions: Scattering and Desorption of NO from Ag(111) and Pt(111), The Journal of Chemical Physics 83 (1985) 2594–2606. doi:10.1063/1.449253.

[95] R. L. Palmer, J. N. Smith, H. Saltsburg, D. R. O'Keefe, Measurements of the Reflection, Adsorption, and Desorption of Gases from Smooth Metal Surfaces, The Journal of Chemical Physics 53 (1970) 1666–1676. doi:10.1063/1.1674242.

[96] J. N. Smith, Scattering of Atomic Beams by Polycrystalline Nickel, The Journal of Chemical Physics 40 (1964) 2520–2527. doi:10.1063/1.1725557.

[97] F. O. Goodman, Review of the theory of the scattering of gas atoms by solid surfaces, Surface Science 26 (1971) 327–362. doi:10.1016/0039-6028(71)90135-X.

[98] J. A. Barker, D. J. Auerbach, Gas-Surface Interactions and Dynamics; Thermal Energy Atomic and Molecular Beam Studies, Technical Report, IBM Research Laboratory, San Jose, California 95193, USA, North-Holland, Amsterdam, 1985.

[99] S. L. Bernasek, G. A. Somorjai, Molecular Beam Scattering from Solid Surfaces, in: Progress in Surface Science, Sidney G. Davison, 1974. URL: https://escholarship.org/uc/item/3tx7g0pv{%}0D.

[100] G. A. Somorjai, S. B. Brumbach, The Interaction Of Molecular Beams With Solid Surfaces, Critical Reviews in Solid State Sciences 4 (1973) 429–454. doi:10.1080/10408437308245837.

[101] M. J. Cardillo, Gas-Surface Interactions Studied with Molecular Beam Techniques, Annual Review of Physical Chemistry 32 (2003) 331–357. doi:10.1146/annurev.pc.32.100181.001555.

[102] W. H. Weinberg, Molecular Beam Scattering from Solid Surfaces, Advances in Colloid and Interface Science 4 (1975) 301–347.

[103] F. C. Hurlbut, On the Molecular Interactions Between Gases and Solids, Technical Report, Institute of Engineering Research, Berkeley, California, 1962.

[104] F. C. Hurlbut, Studies of molecular scattering at the solid surface, Journal of Applied Physics 28 (1957) 844–850. doi:10.1534/genetics.106.069781.

[105] M. N. Bishara, S. S. Fisher, Observed Intensity and Speed Distributions of Thermal-Energy Argon Atoms Scattered from the (111) Face of Silver, The Journal of Chemical Physics 52 (1970) 5661–5675. doi:10.1063/1.1672842.

[106] S. Yamamoto, R. E. Stickney, Molecular Beam Study of the Scattering of Rare Gases from the (110) Face of a Tungsten Crystal, The Journal of Chemical Physics 53 (1970) 1594–1604. doi:10.1063/1.1674218.

[107] V. J. Murray, M. D. Pilinski, E. J. Smoll, M. Qian, T. K. Minton, S. M. Madzunkov, M. R. Darrach, Gas-Surface Scattering Dynamics Applied to Concentration of Gases for Mass Spectrometry in Tenuous Atmospheres, Journal of Physical Chemistry C 121 (2017) 7903–7922. doi:10.1021/acs.jpcc.7b00456.

[108] N. A. Mehta, V. J. Murray, C. Xu, D. A. Levin, T. K. Minton, Nonreactive Scattering of N2 from Layered Graphene Using Molecular Beam Experiments and Molecular Dynamics, Journal of Physical Chemistry C 122 (2018) 9859–9874. doi:10.1021/acs.jpcc.7b11721.

[109] J. P. Moran, H. Y. Wachman, L. Trilling, Scattering of Monoenergetic Argon Beams from Heated Platinum: Planar time-of-Flight Measurements, Physics of Fluids 12 (1969) 987–993. doi:10.1063/1.2163689.

[110] J. N. Smith, H. Saltsburg, Atomic-Beam Scattering from Epitaxially Grown Gold Films, The Journal of Chemical Physics 40 (1964) 3585–3591. doi:10.1063/1.1725056.

[111] L. A. West, E. I. Kozak, G. A. Somorjai, Molecular Beam Scattering from Single Crystal Surfaces under Ultrahigh Vacuum Conditions, Journal of Vacuum Science and Technology 8 (1971) 430–436. doi:10.1116/1.1314479.

[112] R. A. Oman, Numerical Experiments on Scattering of Noble Gases from Single-Crystal Silver, The Journal of

Chemical Physics 48 (1968) 3919–3929. doi:10.1063/1.1669716.

[113] A. G. Stoll, D. L. Smith, R. P. Merrill, Scattering of the Rare Gases (He, Ne, Ar, Kr, and Xe) from Platinum (111) Surfaces, The Journal of Chemical Physics 54 (1971) 163–169. doi:10.1063/1.1674587.

[114] S. S. Fisher, O. F. Hagena, R. G. Wilmoth, Flux and Speed Distributions of Molecular Beams after Scattering by Metal Surfaces, The Journal of Chemical Physics 49 (1968) 1562–1571. doi:10.1063/1.1670279.

[115] M. J. Romney, J. B. Anderson, Scattering of 0.05-5-eV Argon from the (111) plane of silver, The Journal of Chemical Physics 51 (1969) 2490–2496. doi:10.1063/1.1672370.

[116] R. Sau, R. P. Merill, The scattering of Hydrogen, Deuterium, and the rare gases from Silver (111) single crystals, Surface Science 34 (1973) 268–288.

[117] C. T. Rettner, J. A. Barker, D. S. Bethune, Angular and Velocity Distributions Characteristic of the Transition between the Thermal and Structure Regimes of Gas-Surface Scattering, Physical Review Letters 67 (1991) 2183–2186. doi:10.1103/PhysRevLett.67.2183.

[118] W. H. Weinberg, R. P. Merrill, Scattering of Helium, Neon, Argon, Krypton, Xenon, and Deuterium from a Tungsten (110) Surface Characterized by LEED, The Journal of Chemical Physics 56 (1972) 2881–2892. doi:10.1063/1.1677622.

[119] H. Saltsburg, J. N. Smith, Molecular-Beam Scattering from the (111) Plane of Silver, The Journal of Chemical Physics 45 (1966) 2175–2183. doi:10.1063/1.1727905.

[120] B. Berenbak, S. Zboray, B. Riedmuller, D. C. Papageorgopoulos, S. Stolte, A. W. Kleyn, Ar scattering on Ru (0001): a comparison to the washboard model, Physical Chemistry Chemical Physics 4 (2002) 68–74. doi:10.1039/b105514n.

[121] W. A. Alexander, B. S. Day, H. J. Moore, T. R. Lee, J. R. Morris, D. Troya, Experimental and theoretical studies of the effect of mass on the dynamics of gas/organic-surface energy transfer, Journal of Chemical Physics 128 (2008). doi:10.1063/1.2815327.

[122] D. R. Miller, R. B. Subbarao, Scattering of 0.06–2.5-eV Neon and Argon Atoms from a Silver (111) Crystal, The Journal of Chemical Physics 52 (1970) 425–431. doi:10.1063/1.1672701.

[123] A. E. Wiskerke, F. H. Geuzebroek, A. W. Kleyn, B. E. Hayden, A molecular beam study of the O2-Pt(111) interaction, Surface Science 272 (1992) 256–263. doi:10.1016/0039-6028(92)91447-J.

[124] D. R. Miller, R. B. Subbarao, Scattering of 0.06–2.5-eV Neon and Argon Atoms from a Silver (111) Crystal, The Journal of Chemical Physics 52 (1970) 425–431. doi:10.1063/1.1672701.

[125] J. Zhang, D. J. Garton, T. K. Minton, Reactive and inelastic scattering dynamics of hyperthermal oxygen atoms on a saturated hydrocarbon surface, Journal of Chemical Physics 117 (2002) 6239–6251. doi:10.1063/1.1460858.

[126] F. O. Goodman, Three-dimensional hard spheres theory of scattering of gas atoms from a solid surface I. Limit of large incident speed, Surface Science 7 (1967) 391–421. doi:10.1016/0039-6028(67)90029-5.

[127] Y. Watanabe, H. Yamaguchi, M. Hashinokuchi, K. Sawabe, S. Maruyama, Y. Matsumoto, K. Shobatake, Energy transfer in hyperthermal Xe-graphite surface scattering, The European Physical Journal D 38 (2006) 103–109. doi:10.1140/epjd/e2006-00030-6.

[128] J. N. Smith, D. R. O'Keefe, R. L. Palmer, Rare-Gas Scattering from LiF: Correlation with Lattice Properties. II, The Journal of Chemical Physics 52 (1970) 315–320. doi:10.1063/1.1672685.

[129] T. Tomii, T. Kondo, T. Hiraoka, T. Ikeuchi, S. Yagyu, Time-of-flight measurement of molecules rainbow scattered from a LiF (001) surface 112 (2000).

[130] A. Amirav, M. J. Cardillo, P. L. Trevor, L. Carmay, J. C. Tully, Atom – surface scattering dynamics at hyperthermal energies 1796 (1987).